

The chiral and deconfinement crossover transitions: PNJL model beyond mean field *

S. Rößner^a, T. Hell^a, C. Ratti^b and W. Weise^a

^a Physik-Department, Technische Universität München, D-85747 Garching, Germany

^b Department of Physics & Astronomy, State University of New York,
Stony Brook, NY 11794-3800, USA

May 9, 2008

Abstract

The Polyakov loop extended Nambu and Jona-Lasinio model (PNJL model) in a mean field framework shows astonishingly good quantitative agreement with lattice QCD calculations which needs to be better understood. The present work reports on further developments concerning both Polyakov loop and mesonic fluctuations beyond mean field approximation. The evaluation of the thermodynamic potential in Euclidean space-time leads in general to a complex function. The requirement of a strictly real thermodynamic potential constrains the mean field solutions of the PNJL model. In this work we present a way to calculate corrections beyond the mean field results, releasing these constraints and resolving the issues connected to a complex fermion determinant in the PNJL model. We derive a perturbative approach establishing a systematically ordered series of correction terms. The corrections are of special interest for the thermal expectation values of the Polyakov loop $\langle\Phi\rangle$ and its conjugate $\langle\Phi^*\rangle$, for which we find different real values once the quark chemical potential is non-zero. This extension beyond mean field theory is used to review previous results obtained with PNJL models. Explicit calculations show that the corrections introduced, including those from mesonic fluctuations, are small, leading to a convergent procedure.

1 Introduction

Exploring the thermodynamic properties of strongly interacting matter has become a central theme of high-energy nuclear physics in recent years. On the theoretical side, great progress has been achieved thanks to lattice calculations solving discretised QCD numerically. At the present stage a major part of the numerical expense at finite quark chemical potential is caused by the fermion sign problem. The three most promising ways to address this difficulty are multi-parameter re-weighting techniques [1, 2], analytic

*Work supported in part by BMBF, GSI, INFN, the DFG excellence cluster “Origin and Structure of the Universe” and by the Elitenetzwerk Bayern.

continuation from imaginary chemical potentials [3, 4] and Taylor series expansion methods [5–11].

It is an important task of effective field theories and models to reveal principal mechanisms and their functioning behind the otherwise hidden mechanisms of lattice QCD. One approach that successfully describes spontaneous chiral symmetry breaking is the Nambu and Jona-Lasinio (NJL) model. We use the NJL model with $N_f = 2$ quark flavours as one of our starting points. In the NJL model gluonic degrees of freedom are “integrated out”. The role of the gluons is partly modelled by a local effective quark colour current interaction. From this effective interaction a Fierz transformation generates various quark-antiquark and diquark coupling terms. By integrating out the gluons the local $SU(3)_c$ gauge symmetry is lost. As a consequence the NJL model, equipped only with a global $SU(3)_c$ symmetry, does not produce confinement.

To bring aspects of confinement back into the model an additional homogeneous temporal background field with standard $SU(3)_c$ gauge invariant coupling to the quarks is introduced [12, 13], implementing the Polyakov loop. This generalised NJL model, with Polyakov loop dynamics incorporated, is called PNJL model. In the limit of static quarks (i. e. in pure gauge QCD) the Polyakov loop serves as an order parameter for confinement. In this limit the $Z(3)$ centre-symmetry of the $SU(3)_c$ gauge group is unbroken, and the deconfinement transition is connected with the spontaneous breakdown of this symmetry. In the presence of dynamical quarks the $Z(3)$ centre-symmetry is broken explicitly, such that the deconfinement transition is no longer a phase transition in the strict sense. Nevertheless, the Polyakov loop shows a rapid crossover near the deconfinement transition, still permitting to use the Polyakov loop as a measure for deconfinement. The confining gluon dynamics that was lost in the NJL model is now re-introduced via an effective potential. This potential is part of a Ginzburg-Landau model for confinement in the static quark limit. The information necessary in order to specify the effective potential is extracted from pure glue lattice QCD calculations [11], not suffering from the fermion sign problem.

In Sec. 2 we review previous results obtained in the PNJL framework [14, 16–19] at the level of the mean field approximation. In taking steps beyond mean field, it is important to pay special attention to the fermion sign problem which is discussed in Sec. 3. This problem arises in the PNJL model when coupling the Polyakov loop field to the fermionic part of the action. As the Polyakov loop is coupled to the NJL model in analogy to QCD via minimal substitution the fermion sign problem in QCD and in the PNJL model appears on equal footing. The method presented here is a perturbative approach incorporating an expansion about the thermodynamic (large volume) limit. In Sec. 4 the effects of the complex phase of the action on different quantities are investigated. Here the expectation values of the Polyakov loop and its conjugate are of special interest. In the present analysis, the split of the expectation values of the Polyakov loop and its conjugate at non-zero chemical potential arises once fluctuations of the fields are taken into account. Quantities like susceptibilities, in which mean field contributions partially or completely cancel, are sensitive to the corrections beyond mean field, as we shall discuss. Finally in Sec. 5 further corrections beyond Hartree-Fock approximation are estimated. Such contributions to the effective action are generated by mesonic (quark-antiquark) modes that propagate dynamically. The lightest meson mode, the pseudoscalar pion mode with its approximate Nambu-Goldstone character, is the leading correction in this sector. Sec. 6 presents our conclusions and an outlook.

2 The PNJL model

The two-flavour PNJL model including diquark degrees of freedom [20] is derived from the Euclidean action

$$\mathcal{S}_E(\psi, \psi^\dagger, \phi) = \int_0^{\beta=1/T} d\tau \int d^3x \left[\psi^\dagger \partial_\tau \psi + \mathcal{H}(\psi, \psi^\dagger, \phi) \right] + \delta\mathcal{S}_E(\phi, T) \quad (1)$$

with the fermionic Hamiltonian density ¹:

$$\mathcal{H} = -i\psi^\dagger (\vec{\alpha} \cdot \vec{\nabla} + \gamma_4 m_0 - A_4) \psi + \mathcal{V}(\psi, \psi^\dagger), \quad (2)$$

where ψ is the $N_f = 2$ doublet quark field and $m_0 = \text{diag}(m_u, m_d)$ is the quark mass matrix. The quarks move in a background colour gauge field $A_4 = iA_0$, where $A_0 = \delta_{\mu 0} g \mathcal{A}_a^\mu t^a$ with the $SU(3)_c$ gauge fields \mathcal{A}_a^μ and the generators $t^a = \lambda^a/2$. The matrix valued, constant field A_4 relates to the (traced) Polyakov loop as follows:

$$\Phi = \frac{1}{N_c} \text{tr}_c L \quad \text{with } L = \exp \left(i \int_0^\beta d\tau A_4 \right) \quad \text{and } \beta = \frac{1}{T}. \quad (3)$$

In a convenient gauge (the so-called Polyakov gauge), the matrix L is given a diagonal representation

$$L = \exp [i (\phi_3 \lambda_3 + \phi_8 \lambda_8)] . \quad (4)$$

The dimensionless effective fields ϕ_3 and ϕ_8 introduced here are identified with the Euclidean gauge fields in temporal direction, divided by temperature, $A_4^{(3)}/T$ and $A_4^{(8)}/T$. These two fields are a parametrisation of the diagonal elements of $SU(3)_c$. As such the “angles” ϕ_3 and ϕ_8 necessarily have to be real quantities in order to sustain the unitarity of the group. An alternative parametrisation of the diagonal elements of $SU(3)_c$ is given by the Polyakov loop, $\Phi = \frac{1}{3} \text{tr}_c L$, and its conjugate, $\Phi^* = \frac{1}{3} \text{tr}_c L^\dagger$. We define maps between the different parametrisations and diagonal elements as follows

$$\begin{array}{ccc} (\phi_3, \phi_8) \in \mathbb{D}_{\text{gen}} \subset \mathbb{R}^2 & \xrightarrow{h} & (\Phi, \Phi^*) \in \mathbb{D}_{\text{P. loop}} \subset \mathbb{C}^2 \\ & \searrow f_{\text{gen}} \quad \swarrow f_{\text{P. loop}} & \\ & L \in \{U | U \in SU(3)_c \text{ and } U \text{ diagonal}\} & \end{array} \quad (5)$$

All these maps (f_{gen} , $f_{\text{P. loop}}$ and h) and domains \mathbb{D}_{gen} and $\mathbb{D}_{\text{P. loop}}$ can be defined such that f_{gen} , $f_{\text{P. loop}}$ and h are bijective. A naive re-parametrisation of the ϕ_3 - and ϕ_8 -dependence with the Polyakov loop Φ and its conjugate Φ^* can lead to unphysical situations, unless the constraint given by $\mathbb{D}_{\text{P. loop}}$ are implemented carefully such that $L \in SU(3)$ is strictly guaranteed.

The piece $\delta\mathcal{S}_E = \frac{V}{T} \mathcal{U}$ of the action (1) carries information about the gluon dynamics. The potential \mathcal{U} effectively models the confinement-deconfinement transition and the region up to temperatures of roughly $T \lesssim 2T_c$ in quarkless, pure gauge QCD on the mean field Ginzburg-Landau level. At temperatures very far above the transition a description of the thermodynamics with just the two order parameters Φ and Φ^* is not appropriate as transverse gluons will become important. Transverse gluon degrees of freedom cannot be described by Polyakov loops.

¹ $\vec{\alpha} = \gamma_0 \vec{\gamma}$ and $\gamma_4 = i\gamma_0$ in terms of the standard Dirac γ matrices.

The Polyakov loop is an order parameter for confinement in SU(3) gauge theory. In the confined low temperature phase the expectation value of the Polyakov loop vanishes, $\langle \Phi \rangle = 0$, while $\langle \Phi \rangle \neq 0$ implies deconfinement. Let T_0 be the critical temperature separating the two phases. As previously mentioned the symmetry which is restored at $T < T_0$ and broken above T_0 is the Z(3) centre-symmetry of SU(3)².

Therefore, the Landau effective potential describing the dynamics, the Polyakov loop potential $\mathcal{U}(\Phi, T)$, has to be Z(3) symmetric in Φ . The basic building blocks for such a potential are $\Phi^* \Phi$, Φ^3 and Φ^{*3} terms. The potential used here differs from the simplest ansatz generating a first order phase transition as it is implemented in [14]. Instead we use the ansatz given in [20, 21] motivated by the SU(3) Haar measure:

$$\frac{\mathcal{U}(\Phi, \Phi^*, T)}{T^4} = -\frac{1}{2}a(T) \Phi^* \Phi + b(T) \ln \left[1 - 6 \Phi^* \Phi + 4 \left(\Phi^{*3} + \Phi^3 \right) - 3 (\Phi^* \Phi)^2 \right] , \quad (6)$$

where the temperature dependent prefactors are given by

$$a(T) = a_0 + a_1 \left(\frac{T_0}{T} \right) + a_2 \left(\frac{T_0}{T} \right)^2 \quad \text{and} \quad b(T) = b_3 \left(\frac{T_0}{T} \right)^3 . \quad (7)$$

The logarithmic divergence near $\Phi^*, \Phi \rightarrow 1$ properly constrains the Polyakov loop to values attainable by the normalised trace of an element of SU(3). The parameters of $\mathcal{U}(\Phi, \Phi^*, T)$ are chosen such that the critical temperature of the first order transition is indeed equal to T_0 (fixed at 270 MeV [24]) and that $\Phi^*, \Phi \rightarrow 1$ as $T \rightarrow \infty$.

The numerical values using these constraints are taken as given in Refs. [20, 21]

$$a_0 = 3.51 , \quad a_1 = -2.47 , \quad a_2 = 15.2 , \quad b_3 = -1.75 .$$

The resulting uncertainties are estimated to be about 6% for a_1 , less than 3% for a_2 and 2% for b_3 . The value $a_0 = \frac{16\pi^2}{45}$ chosen here reproduces the Stefan-Boltzmann limit. This is not mandatory, of course, since the high-temperature limit is governed by (transverse) gluonic degrees of freedom not covered by the Polyakov loop which represents the longitudinal gauge field. Alternative parametrizations of \mathcal{U} are possible, such as the two-parameter form guided by the strong-coupling approach [13], which has a different high temperature limit. In the present context these differences are not crucial as we systematically restrict ourselves to temperatures close to the transition region, $T \lesssim 2T_c$, where different forms of \mathcal{U} give remarkably similar results as pointed out in Ref. [22].

In Fig. 1 we plot the Polyakov loop potential using the parametrisation given in Refs. [20, 21] at $T = T_0 = 0.27 \text{ GeV}$. This illustrates the Z(3) symmetry and how the single minimum at $T < T_0$ becomes degenerate with three minima at $T = T_0$. Above T_0 only these three minima survive. Of course upon spontaneous breakdown of the Z(3) centre-symmetry, the three minima and the Z(3) centre-symmetry of the potential remain intact even though the vacuum expectation value does no longer show the symmetry of the potential.

The interaction \mathcal{V} in Eq. (2) includes chiral SU(2) \times SU(2) invariant four-point couplings of the quarks acting in pseudoscalar-isovector/scalar-isoscalar quark-antiquark and scalar diquark channels:

$$\mathcal{V} = -\frac{G}{2} \left[(\bar{\psi} \psi)^2 + (\bar{\psi} i \gamma_5 \vec{\tau} \psi)^2 \right] - \frac{H}{2} \left[(\bar{\psi} \mathcal{C} \gamma_5 \tau_2 \lambda_2 \bar{\psi}^T) (\psi^T \gamma_5 \tau_2 \lambda_2 \mathcal{C} \psi) \right] , \quad (8)$$

²The centre of SU(3) contains all those SU(3) elements that commute with all other SU(3) elements, i. e. the elements $e^{i \frac{2\pi}{3} k} \mathbb{1}$, with $k \in \mathbb{Z}$ constituting a Z(3) subgroup of SU(3).

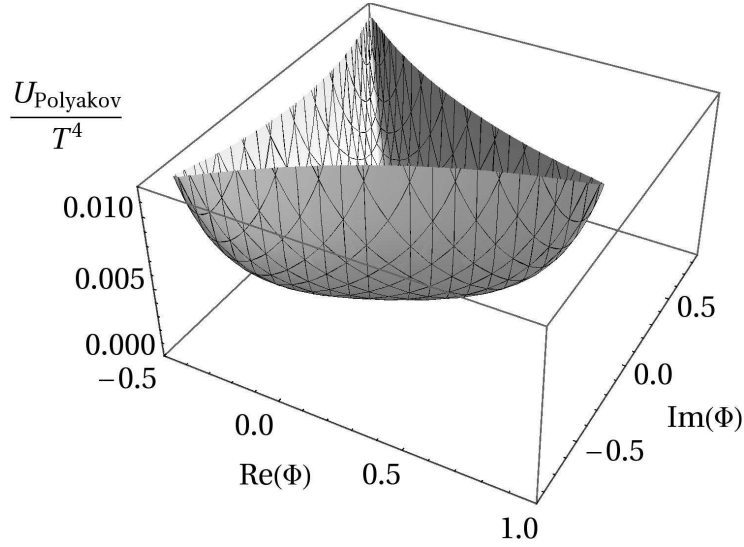


Figure 1: The Polyakov loop potential $\mathcal{U}(\Phi, \Phi^*, T)/T^4$ plotted in the complex plane of Φ at $T = T_0 = 0.27 \text{ GeV}$.

where \mathcal{C} is the charge conjugation operator. The interaction terms in Eq. (8) are obtained from a local colour current-current interaction between quarks,

$$\mathcal{L}_{\text{int}} = -G_c(\bar{\psi}\gamma_\mu t^a \psi)(\bar{\psi}\gamma^\mu t^a \psi) ,$$

by a Fierz transformation which relates the coupling strengths G and H as $G = \frac{4}{3}H$, which we choose not to alter³.

The NJL model with two quark flavours is usually modelled with three parameters, a current quark mass $m_{u,d}$, a local four quark coupling strength G and a three momentum cutoff Λ . The parameters used here are the ones used in [14, 20, 21]:

$$m_{u,d} = 5.5 \text{ MeV} , \quad G = \frac{4}{3}H = 10.1 \text{ GeV}^{-2} , \quad \Lambda = 0.65 \text{ GeV} ,$$

fixed to reproduce the pion mass and decay constant in vacuum and the chiral condensate as $m_\pi = 139.3 \text{ MeV}$, $f_\pi = 92.3 \text{ MeV}$ and $\langle \bar{\psi}_u \psi_u \rangle = -(251 \text{ MeV})^3$.

To evaluate the thermodynamic properties of the model the quark degrees of freedom are integrated out. New auxiliary fields are introduced by bosonisation, absorbing quark-antiquark and quark-quark (antiquark-antiquark) correlations. These are a scalar-pseudoscalar field $(\sigma, \vec{\pi})$ and a diquark (antidiquark) field Δ (Δ^*). The resulting thermodynamic potential then reads

$$\Omega_0 = \frac{T}{V} \mathcal{S}_{\text{bos}} = \mathcal{U}(\Phi, \Phi^*, T) - \frac{T}{2} \sum_n \int \frac{d^3 p}{(2\pi)^3} \text{Tr} \ln \left[\beta \tilde{S}^{-1}(i\omega_n, \vec{p}) \right] + \frac{\sigma^2}{2G} + \frac{\Delta^* \Delta}{2H} , \quad (9)$$

where the Matsubara sum runs over $\omega_n = (2n+1)\pi T$ reproducing antiperiodic boundary conditions in the Euclidean time direction. The inverse Nambu-Gor'kov propagator \tilde{S}^{-1}

³Additional terms generated by the Fierz transformation are of no importance in the present context and will be omitted.

in Eq. (9) is defined by

$$\tilde{S}^{-1}(i\omega_n, \vec{p}) = \begin{pmatrix} i\gamma_0 \omega_n - \vec{\gamma} \cdot \vec{p} - m + \gamma_0 (\mu - iA_4) & \Delta\gamma_5 \tau_2 \lambda_2 \\ -\Delta^* \gamma_5 \tau_2 \lambda_2 & i\gamma_0 \omega_n - \vec{\gamma} \cdot \vec{p} - m - \gamma_0 (\mu - iA_4) \end{pmatrix}. \quad (10)$$

The mass of the quark-quasiparticles is given as in the standard NJL model by the gap equation

$$m = m_0 - \langle \sigma \rangle = m_0 - G \langle \bar{\psi} \psi \rangle. \quad (11)$$

The Matsubara sum is evaluated analytically. The quasiparticle energies emerging in this procedure are related to the solutions of $\det [\tilde{S}^{-1}(p_0)] = 0$. The bosonised action then reads

$$\begin{aligned} \frac{T}{V} \mathcal{S}_{\text{bos}} = & \mathcal{U}(\Phi, \Phi^*, T) + \frac{\sigma^2}{2G} + \frac{\Delta^* \Delta}{2H} \\ & - 2N_f \int \frac{d^3 p}{(2\pi)^3} \sum_j \left\{ T \ln [1 + e^{-E_j/T}] + \frac{1}{2} \Delta E_j \right\}, \end{aligned} \quad (12)$$

with six distinct quasiparticle energies

$$\begin{aligned} E_{1,2} &= \varepsilon(\vec{p}) \pm \tilde{\mu}_b, \\ E_{3,4} &= \sqrt{(\varepsilon(\vec{p}) + \tilde{\mu}_r)^2 + |\Delta|^2} \pm iT\phi_3, \\ E_{5,6} &= \sqrt{(\varepsilon(\vec{p}) - \tilde{\mu}_r)^2 + |\Delta|^2} \pm iT\phi_3, \end{aligned} \quad (13)$$

where $\varepsilon(\vec{p}) = \sqrt{\vec{p}^2 + m^2}$. Additionally we have introduced

$$\tilde{\mu}_b = \mu + 2iT \frac{\phi_8}{\sqrt{3}}, \quad \tilde{\mu}_r = \mu - iT \frac{\phi_8}{\sqrt{3}}. \quad (14)$$

The energy difference ΔE_j is defined as the difference of the quasiparticle energy and the energy of a free fermion, $\varepsilon_0 = \sqrt{\vec{p}^2 + m_0^2}$: $\Delta E_j = E_j - \varepsilon_0 \pm \mu$.

The form of the bosonised action, Eq. (12), does not allow to factor out the Polyakov loop fields Φ and Φ^* , as it was done in Ref. [14]. Instead we keep the form of Eq. (12) using ϕ_3 and ϕ_8 with $\phi_3, \phi_8 \in \mathbb{D}_{\text{gen}}$, where \mathbb{D}_{gen} has to be understood in the context of Eq. (5). The parameter space of ϕ_3 and ϕ_8 is periodic. To obtain an injective mapping f_{gen} in Eq. (5), \mathbb{D}_{gen} must only contain one such period.⁴

Constraints imposed by mean field approximation

We would like to add some notes concerning our terminology before we go on with the presentation of this work. One aspect of the mean field approximation is that only spatially and temporally constant fields are used. Other degrees of freedom are integrated out. Usually the process of integrating out spatially and temporally fluctuating parts is achieved by neglecting terms in the action that couple to such fluctuating parts. It is

⁴We use the domain defined by $\mathbb{D}_{\text{gen}} = \left\{ \left(\phi_8 \geq -\frac{\pi}{\sqrt{3}} \right) \wedge \left(\phi_8 \leq \sqrt{3}(\phi_3 + \frac{2\pi}{3}) \right) \wedge \left(\phi_8 \leq \sqrt{3}(-\phi_3 + \frac{2\pi}{3}) \right) \right\}$. Note that \mathbb{D}_{gen} is not the periodic domain of L but only of Φ . The periodic domain of L is larger than the one of Φ , as Φ is invariant under exchange of different colours by virtue of the trace's invariance under unitary transformations of L .

quite common to carry the mean field approximation even further: apart from taking into account only spatially and temporally constant fields, only a single field configuration of the zero-momentum mode is used to approximate the path integral, namely the classical trajectory. This trajectory is equivalent to the thermodynamic expectation value. With this definition, the path integral in mean field approximation becomes trivial, while the standard action is promoted to a Landau effective action. The action is minimised by varying the classical fields over the *physically meaningful* range to find the configuration with the largest contribution to the approximated integral.⁵ In the PNJL model *physically meaningful* means in particular that ϕ_3 and ϕ_8 are real fields, satisfying the group theoretical constraints mentioned previously. We define the mean field thermodynamic potential by

$$\Omega_{\text{MF}} \equiv \Omega_0 = \frac{T}{V} \mathcal{S}_{\text{bos}}. \quad (15)$$

The necessary condition for the minimisation of the effective action or the mean field thermodynamic potential in a standard situation is

$$\frac{\partial \Omega_{\text{MF}}}{\partial (\sigma, \Delta, \phi_3, \phi_8)} = 0. \quad (16)$$

However, in the PNJL case this statement is incomplete as it stands. A physically meaningful thermodynamic potential must be a real-valued function whereas \mathcal{S}_{bos} of Eqs. (9, 12) is complex. The complex values emerge from the fermion sign problem founded in the non-positive definite inverse fermion propagator of the model once the chemical potential μ is different from zero.⁶

The definition of mean field approximation as given at the beginning of this subsection requires to restrict all quantities to physically meaningful values. The optimal choice under this restriction is to select the most important field configuration. This is the one for which $|e^{-\mathcal{S}_{\text{E}}}|$ is maximal.⁷ With $\mathcal{S}_{\text{E}} = \mathcal{S}_{\text{bos}}$ this is equivalent to minimising $\text{Re}[\mathcal{S}_{\text{bos}}]$, which through Eq. (15) implies the necessary conditions

$$\frac{\partial \text{Re}[\Omega_{\text{MF}}]}{\partial (\sigma, \Delta, \phi_3, \phi_8)} = 0. \quad (17)$$

Additionally, it has to be ensured that the resulting field configuration solving Eq. (17) leads to a real-valued thermodynamic potential.

A procedure applied in previous publications [14, 16–19] is to demand that $\Omega \in \mathbb{R}$ while the (a priori real) fields are left floating in the complex plane. The variables ϕ_3 and ϕ_8 were substituted by the Polyakov loop Φ and its conjugate Φ^* , while not taking care of the uniqueness of the mappings in Eq. (5). As it stands, this procedure is not consistent with the underlying group constraints and leads to unphysical complex values for ϕ_3 and ϕ_8 .

⁵At this point we do not assume any analytic properties of the action as a function of the fields. The saddle point approximation which uses an analytic continuation of the action into the space of complex (instead of real) fields is not considered here. A discussion and comparison of the approach presented in this work with the saddle point approximation is given in Sec. 3.2.

⁶The fermion sign problem in QCD emerges in exactly the same way, as the background loop field is coupled in analogy to the minimal substitution in QCD.

⁷In analogy to the procedure in Minkowskian space-time one might argue that the complex phase needs to become stationary. Taking the thermodynamic limit one observes that the stationary phase field configuration is favoured over any other configuration by the factor $\frac{V}{T}$, while the absolute value is favoured over other configurations by a factor $e^{\frac{V}{T}}$.

It can be justified, however, in a broader mean field context if the action features analytic properties allowing the saddle point approximation, as discussed in Ref. [23].

The combination of the restrictions $\Omega \in \mathbb{R}$ and $\phi_3, \phi_8 \in \mathbb{R}$ allow only certain limited configurations of ϕ_3 and ϕ_8 . The condition $\phi_3, \phi_8 \in \mathbb{R}$ implies in mean field approximation that, due to Eq. (4), Φ and Φ^* are the complex conjugates of each other, and we find in mean field theory $\langle \Phi \rangle_{\text{MF}} = \Phi_{\text{MF}}$ and $\langle \Phi^* \rangle_{\text{MF}} = \Phi_{\text{MF}}^*$. At $\mu = 0$ the Polyakov loop Φ and its complex conjugate Φ^* are treated equally due to the charge conjugation invariance of the model. This immediately implies $\Phi_{\text{MF}} = \Phi_{\text{MF}}^* \in \mathbb{R}$ in mean field approximation, fixing $\phi_8 = 0$. The values of the derivative $\frac{\partial \Omega_{\text{MF}}}{\partial \phi_8}$ at $\phi_8 = 0$ are purely imaginary. Therefore $\phi_8 = 0$ satisfies Eq. (17). The effective Polyakov loop potential $\mathcal{U} = \mathcal{U}(T, \Phi, \Phi^*)$ in its parametrisation (6) is minimal for $\Phi = \Phi^*$ at fixed $|\Phi|$. We find that the Polyakov loop potential \mathcal{U} is always strong enough to keep $\Phi = \Phi^*$ or, equivalently, to keep $\phi_8 = 0$. Not all parametrisations of \mathcal{U} will maintain this solution. If the curvature of the potential \mathcal{U} is not strong enough, the solution $\phi_8 = 0$ becomes unstable, and $\phi_8 = 0$ is the position of a local maximum of the potential. In Ref. [16] a symptom of this fact has been described: the susceptibility of $\text{Re } \Phi$ may become negative. The potential used in the present work does not show such deficiencies.

Chiral and deconfinement transitions

At this point it is instructive to examine how chiral and Polyakov loop dynamics cooperate to produce crossover transitions (at zero chemical potential) which end up in a narrow overlapping range of temperatures (see Fig. 2). In isolation, the pure gauge Polyakov loop sector and the NJL sector in the chiral limit show first (second) order phase transitions with critical temperatures far separated. When entangled in the PNJL model, these transitions (with non-zero quark masses) move together to form a joint crossover pattern.

3 The complex form of the action

When integrating out the quark fields the non-hermitian term $i\gamma_0 A_4$ in the inverse quark propagator of the bosonised action leads to a formally complex effective action.⁸ As discussed in the previous section, treating such a complex action in mean field approximation as it is understood here, is tantamount to ignoring imaginary parts of the thermodynamic potential. On the other hand, the behaviour under charge conjugation of the quantities of interest allows to show that all these thermodynamic quantities should in fact be strictly real [23]. This suggests that it is our mean field approximation scheme that introduces restricting constraints. We shall therefore present a method to refine the mean field approximation to recover all originally accessible degrees of freedom. In the section below we present such a method that is able to systematically improve the mean field result order by order.

⁸This is an effective action with respect to the fermion fields that have been integrated out; it is not an effective action with respect to the gluon mean field A_4 , and with respect to the auxiliary quasiparticle fields that have been introduced in the bosonisation procedure. In fact, when reducing the field dependence to spatially constant fields we have assumed that these fields are approximate order parameters. In this approximation the action is treated like a Landau effective action.

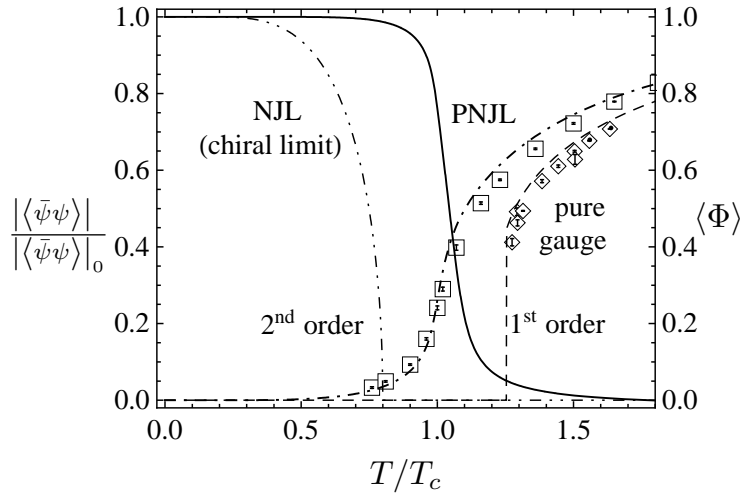


Figure 2: The dash-dot-dotted line and the dashed line give the strength of the chiral condensate in the NJL model (with massless quarks) and the size of the Polyakov loop in the pure gauge model. Joining the Polyakov loop to the NJL model (now with non-zero quark masses) using minimal substitution couples chiral and Polyakov loop crossovers. The resulting chiral condensate (solid) and the Polyakov loop (dash-dotted) in the PNJL model at mean field level are shown as calculated. For comparison lattice data for the Polyakov loop in pure-gauge and full QCD (including quarks) are also shown [25]

3.1 Gaussian approximation of the PNJL action

In order to construct an effective action the boson field variables need to be integrated out as well. In general this cannot be done analytically. A frequently used procedure is to expand the effective action with respect to the fermionic fields up to second order and truncate. We define the expansion coefficients ω_i by

$$\mathcal{S}_{\text{bos}} \approx \mathcal{S}_{\text{trunc}} = \frac{V}{T} \left(\omega_0 + \omega_1 \cdot \xi + \frac{1}{2} \xi \cdot \omega_2 \cdot \xi \right) . \quad (18)$$

Here ξ generically stands for all bosonic fields that have not been integrated out. We furthermore use the notation $a \cdot b = \sum_i a_i b_i$, where i enumerates all bosonic degrees of freedom to be integrated over, and correspondingly we use $a \cdot A \cdot b = \sum_{ij} a_i A_{ij} b_j$. The fields ξ are calculated from the original fields, θ , via $\xi = \theta - \theta_0$, where θ_0 is the mean field value of θ , i.e. the point about which the action \mathcal{S}_{bos} is expanded.

The expansion is performed such that the path integral is optimally approximated. This is achieved when the truncated terms in the expansion of the action are maximally suppressed. The expansion is controlled by the Gaussian $e^{-\mathcal{S}_{\text{trunc}}}$. With $e^{-\mathcal{S}_{\text{trunc}}} \in \mathbb{C}$ the approximation is optimal near the maximum of $|e^{-\mathcal{S}_{\text{trunc}}}|$. The equations to determine θ_0 are the mean-field equations (17),

$$\frac{\partial \text{Re}[\mathcal{S}_{\text{bos}}]}{\partial \theta} = 0 , \quad (19)$$

(also used in a preceeding paper [20]), i.e. $\theta_0 = \theta_{\text{MF}}$.

With this expansion, truncated after the second order, the integral over the fields

$$\int \cdots \int_{-\infty}^{\infty} d\xi e^{-\mathcal{S}_{\text{bos}}} \approx \int \cdots \int_{-\infty}^{\infty} d\xi e^{-\mathcal{S}_{\text{trunc}}} = e^{-\mathcal{S}_{\text{Gauss}}} \quad (20)$$

is Gaussian and can be performed analytically. Note that in the first order term of the expansion with respect to the fields, ω_1 is purely imaginary as ξ is the difference of the field to the mean field result.⁹ Therefore the integral in Eq. (20) has the form of a Fourier integral. We identify $k = \text{Im}[\frac{V}{T}\omega_1]$ or $k = \frac{V}{iT}\omega_1$. Using well-known Fourier transforms we find

$$e^{-\mathcal{S}_{\text{Gauss}}} = \frac{1}{\mathcal{N}} \exp \left\{ -\frac{V}{T}\omega_0 - \frac{T}{2V} k \cdot [\omega_2]^{-1} \cdot k \right\} \Big|_{k=\frac{V}{iT}\omega_1}. \quad (21)$$

The evaluation of thermal expectation values simplifies if one considers the action as a function of the Fourier variable k . We define

$$Z(k) = [e^{-\mathcal{S}_{\text{Gauss}}}] (k) = \frac{1}{\mathcal{N}} \exp \left\{ -\frac{V}{T}\omega_0 - \frac{T}{2V} k \cdot [\omega_2]^{-1} \cdot k \right\}. \quad (22)$$

The normalisation factor \mathcal{N} can be obtained from the Fourier transform:

$$\mathcal{N} = \left(\frac{V}{2\pi T} \right)^{\frac{N}{2}} |\det [\omega_2]|^{\frac{1}{2}}, \quad (23)$$

where N is the number of boson fields considered.

The next step is to consider the action in Gaussian approximation using an expansion in $\frac{T}{V}$ about zero, i.e. in an expansion about the thermodynamic limit. For small $\frac{T}{V}$, the contribution of the normalisation \mathcal{N} to the effective action can be neglected, as this contribution ($\ln \mathcal{N}$) depends only logarithmically on $\frac{V}{T}$, while the leading order terms of $\mathcal{S}_{\text{Gauss}}$ are proportional to $\frac{V}{T}$. In the following it is always this limit we are interested in.¹⁰ This allows to write the effective action in Gaussian approximation as

$$\mathcal{S}_{\text{Gauss}}(k) = \frac{V}{T}\omega_0 + \frac{T}{2V} k \cdot [\omega_2]^{-1} \cdot k. \quad (24)$$

3.2 Corrections to the mean field equations

The following derivation is based on solutions of the mean field equations (19). Leading corrections to these solutions can be constructed by considering not only the solution itself, but also its neighbourhood. The thermal expectation values now incorporate more field configurations than in mean field. In this approximation of the path integral the fields are fluctuating according to the statistical weight determined by the exponential of the action. In this sense the fields can be fluctuating even though still constant in space and imaginary time. We use Eq. (24) to derive such corrections to the thermal expectation values. These

⁹In Eq. (19) only the real part of the mean field thermodynamic potential was minimised such that there may still be imaginary gradients.

¹⁰If one considers a finite volume at finite temperature the logarithm of the normalisation \mathcal{N} becomes important as soon as the second derivative ω_2 is close to singular. In this case the second term in Eq. (24) is negligible. Higher order corrections discussed below will also vanish, i.e. the potential is locally flat. $\ln \mathcal{N}$ will however become large. Physically this situation appears close to a critical point where the correlation lengths start to diverge and reach the order of $V^{\frac{1}{3}}$. For $V \rightarrow \infty$ this only happens exactly at the critical point.

first corrections are generated by the linear imaginary and quadratic (Gaussian) terms of the action. Further corrections can be derived from the “interaction” $\mathcal{S}_{\text{bos}} - \mathcal{S}_{\text{trunc}}$. Both types of corrections will be ordered by their formal size, establishing a systematic perturbative expansion.

In Sec. 5 below we also discuss the influence of fully dynamic fluctuations, i.e. fluctuations of fields that are not constant in space and imaginary time. In that later section we will focus on pion and sigma fluctuations, the ones of prime importance in this context.

Gaussian approximation

Thermodynamic expectation values are calculated in the Gaussian approximation via the path integral formalism¹¹

$$\langle f \rangle = \frac{1}{\mathcal{N}} \int \cdots \int_{-\infty}^{\infty} d\xi f(\xi) e^{-\mathcal{S}_{\text{trunc}}(\xi)}, \quad (25)$$

with $\mathcal{S}_{\text{trunc}}$ given by Eq. (18). The Fourier transformation involves the replacement $\xi \rightarrow i\partial_k$ so that Eq. (25) can now be written with the help of Eqs. (20, 21, 22):

$$\langle f \rangle = \frac{1}{Z(k)} [f(i\partial_k) Z(k)] \Big|_{k=\frac{V}{iT}\omega_1}. \quad (26)$$

The applied rationale is analogous to the generating functional formalism. Note again that ξ is defined as the difference of the field configuration and its mean field value, $\theta - \theta_{\text{MF}}$, which implies that $f(0)$ is just the mean field result. As ξ is an N -dimensional vector of all field degrees of freedom, k as well is an N -dimensional vector.

Thermodynamic potential

Now that the corrections in Gaussian approximation due to the complex structure of the action are under control, corrections coming from the neglected part of the action $\mathcal{S}_{\text{bos}} - \mathcal{S}_{\text{trunc}}$ have to be worked out. To do this the exponential of this part of the action, $e^{-(\mathcal{S}_{\text{bos}} - \mathcal{S}_{\text{trunc}})}$, is treated formally as a part of the function f in Eq. (25). In general, this split of \mathcal{S}_{bos} into $\mathcal{S}_{\text{trunc}}$ and $\mathcal{S}_{\text{bos}} - \mathcal{S}_{\text{trunc}}$ does not change the path integral.

In a first step $f(\xi) e^{-(\mathcal{S}_{\text{bos}} - \mathcal{S}_{\text{trunc}})}$ is expanded in powers of ξ . Each power of ∂_k provides us with a factor $\frac{T}{V}$, with k defined as $k = \frac{V}{iT}\omega_1$. These factors are, however, compensated whenever ∂_k acts directly on the exponential factor of $Z(k)$, producing a factor $\delta = \frac{T}{V} [\omega_2]^{-1} \cdot k$. We establish an expansion in $\frac{T}{V}$ and δ which provides a convenient approximation scheme when both $\frac{T}{V}$ and δ are small. In case of $\frac{T}{V}$ this is easy to achieve as we are interested in the thermodynamic limit. The size of δ , however, is controlled by the action itself; whether the expansion in δ is justified or not depends on the model. The explicit calculations presented below will show that in the present version of the PNJL model the expansion in δ is a good approximation.

It is now possible to write down the thermal expectation value of a generic function f as an expansion in powers of $\frac{T}{V}$ and δ . We proceed here in analogy to the Feynman diagram formalism established for perturbation theories. In perturbation theory we consider an action \mathcal{S} that is typically split into a free part \mathcal{S}_0 and an interaction part \mathcal{S}_I . Here the

¹¹The number of bosonic degrees of freedom left in this effective model is N such that a path integral is reduced to an N -dimensional integral.

free part is just the action in Gaussian approximation, the term including the residual imaginary gradient of the action is treated as a source term in the context of the generating functional formalism. We write generically

$$Z = \frac{1}{\mathcal{N}} \int \mathcal{D}\xi e^{-\mathcal{S}} = \frac{1}{\mathcal{N}} \int \mathcal{D}\xi e^{-\mathcal{S}_0} \sum_{l=0}^{\infty} \frac{1}{l!} (-\mathcal{S}_I)^l. \quad (27)$$

If only corrections to the partition function of the PNJL model are to be calculated the interaction part \mathcal{S}_I of the action in Eq. (27) is identified with $\mathcal{S}_{\text{bos}} - \mathcal{S}_{\text{trunc}}$. With this in mind we can establish the following Feynman rules:

$$\begin{aligned} \begin{array}{c} \times \\ \hline j \end{array} &= -\frac{\partial \mathcal{S}_{\text{bos}}}{\partial \xi_j} & \begin{array}{c} \longrightarrow \\ j \quad k \end{array} &= + \left[\frac{\partial^2 \mathcal{S}_{\text{bos}}}{\partial \xi_j \partial \xi_k} \right]^{-1} \\ \begin{array}{c} k \\ \diagup \\ \bullet \\ \diagdown \\ j \quad l \end{array} &= -\frac{\partial^3 \mathcal{S}_{\text{bos}}}{\partial \xi_j \partial \xi_k \partial \xi_l} & \begin{array}{c} l \\ | \\ j \quad \bullet \quad m \\ | \\ k \end{array} &= -\frac{\partial^4 \mathcal{S}_{\text{bos}}}{\partial \xi_j \partial \xi_k \partial \xi_l \partial \xi_m} \\ \vdots & & \vdots & \end{aligned} \quad (28)$$

Note that the propagator in Eq. (28) comes with a “+” sign, while the other terms come with a “−” sign. What is needed to use these rules systematically is a scheme that orders all possible diagrams according to their importance. There are two small quantities available here to establish rules of importance, $\frac{T}{V}$ and δ .

First consider the thermodynamic expansion using $\frac{T}{V}$ as an expansion parameter. All diagrams shown in Eq. (28) except the one for the propagator are proportional to $\frac{V}{T}$ as the action is an extensive quantity. The propagator in Eq. (28) is proportional to $\frac{T}{V}$. The leading order in the thermodynamic expansion therefore must contain $n - 1$ propagators if there are n elements in the diagram different from a propagator. This immediately implies that the leading order correction to the mean field result in the thermodynamic expansion does not contain any loop diagrams. Secondly, we consider the expansion in the parameter δ , which is the composite of the two elements in the first line of Eq. (28) and does not come with a $\frac{T}{V}$ -dependence.

In perturbation theory it can be shown that only connected diagrams contribute to the partition function, i. e. that

$$Z_I = \langle e^{-\mathcal{S}_I} \rangle_0 = \sum_{l=0}^{\infty} \frac{1}{l!} \langle (-\mathcal{S}_I)^l \rangle_0 = \exp \left\{ \sum_{n=1}^{\infty} \frac{1}{n!} \langle (-\mathcal{S}_I)^n \rangle_{0c} \right\}, \quad (29)$$

where $\langle \cdots \rangle_0$ is the expectation value with respect to the unperturbed action, and $\langle \cdots \rangle_{0c}$ is the expectation value of the connected diagrams with respect to the unperturbed action. Note that here the corrections depicted by the Feynman diagrams are corrections to the negative action, $-\mathcal{S}$, as the partition function was defined by $Z = e^{-\mathcal{S}_{\text{eff}}}$. The corrections therefore need to be subtracted from the mean field result of the action \mathcal{S}_{MF} .

Thermodynamic expectation values

For the thermal expectation values of f we write

$$\langle f \rangle = \langle f e^{-\mathcal{S}_I} \rangle_0 = \sum_{l=0}^{\infty} \frac{1}{l!} \langle f (-\mathcal{S}_I)^l \rangle_0. \quad (30)$$

Here each term under the sum can be written in terms of connected expectation values

$$\begin{aligned} \langle f(-\mathcal{S}_I)^l \rangle_0 = & \sum_{a_1, a_2, \dots, a_n, m=0}^{\infty} \frac{l!}{a_1! a_2! (2!)^{a_2} \dots (n!)^{a_n} m!} \langle (-\mathcal{S}_I^1) \rangle_{0c}^{a_1} \langle (-\mathcal{S}_I^2) \rangle_{0c}^{a_2} \dots \\ & \dots \langle f(-\mathcal{S}_I^m) \rangle_{0c} \delta_{a_1+2a_2+\dots+na_n+m, l}. \end{aligned} \quad (31)$$

Substituting back in Eq. (30) gives

$$\langle f e^{-\mathcal{S}_I} \rangle_0 = \exp \left\{ \sum_{n=1}^{\infty} \frac{1}{n!} \langle (-\mathcal{S}_I)^n \rangle_{0c} \right\} \times \sum_{m=0}^{\infty} \frac{1}{m!} \langle f(-\mathcal{S}_I)^m \rangle_{0c}. \quad (32)$$

Using Eq. (29) we find the final result

$$\langle f \rangle = \langle f e^{-\mathcal{S}_I} \rangle_0 = \sum_{n=0}^{\infty} \frac{1}{n!} \langle f(-\mathcal{S}_I)^n \rangle_{0c}. \quad (33)$$

In terms of Feynman diagrams Eq. (33) can be translated into all those connected diagrams that contain exactly one insertion coming from the function f . The Feynman rules for the insertions of f are

$$\begin{aligned} \text{---} \circ \text{---} \quad j &= \frac{\partial f}{\partial \xi_j} & \text{---} \circ \text{---} \quad j \quad k &= \frac{\partial^2 f}{\partial \xi_j \partial \xi_k} \\ \begin{array}{c} k \\ \diagup \\ \circ \text{---} l \\ \diagdown \\ j \end{array} &= \frac{\partial^3 f}{\partial \xi_j \partial \xi_k \partial \xi_l} & \begin{array}{c} l \\ | \\ \circ \text{---} m \\ | \\ j \quad k \end{array} &= \frac{\partial^4 f}{\partial \xi_j \partial \xi_k \partial \xi_l \partial \xi_m} \\ \vdots & & \vdots & \end{aligned} \quad (34)$$

The ordering of the Feynman graphs proceeds in analogy to the correction of the action. As one insertion of f has to be included into the graph the lowest order in $\frac{T}{V}$ is now $(\frac{T}{V})^0 = \text{const.}$ as anticipated. The lowest order corrections in $\frac{T}{V}$ and δ are shown in Table 1.

Writing $\langle f \rangle$ as in Eq. (26), neglecting corrections of the interaction part of the action \mathcal{S}_I , the lowest order in the thermodynamic expansion (terms $\propto (T/V)^0$) can be summed up by substituting the argument θ of the function f by $\theta_0 + \delta\theta$, where $\delta\theta$ is the lowest order correction of the fields θ (see Tab. 1, $\alpha = 0$ and $\beta = 1$): $\langle f \rangle_{\text{part. sum}} = f(\theta_0 + \delta\theta)$. This partial summation is exact in the orders $\alpha = 0$ and $\beta = 0, 1$. It will be used below in the numerical calculations of $\langle \Phi \rangle$ and $\langle \Phi^* \rangle$.

The modified self consistency constraints

A useful consistency check, performed here only to lowest order, is to verify that the thermal expectation values are now closer to the properties of an order parameter than the mean field result. In other words: we examine whether the thermodynamic potential Ω is a Landau effective action minimised with respect to $\langle \sigma \rangle$, $\langle \Delta \rangle$, $\langle \Phi \rangle$, $\langle \Phi^* \rangle$ using Eq. (33) for the expectation values. The analysis below is done for the lowest order terms, $\alpha = 0$ and $\beta = 0, 1$. We start from the form also used for the numerical calculations, presented below Eq. (39), and differentiate with respect to the expectation values

$\langle \theta \rangle = (\langle \sigma \rangle, \langle \Delta \rangle, \langle \Phi \rangle, \langle \Phi^* \rangle)^T$. To orders $\alpha = 0$ and $\beta = 0, 1$ we find that $\langle \theta \rangle = \theta_0 + \delta\theta$, where $\delta\theta$ is given by

$$\delta\theta_i = \frac{1}{2} \left(\left[\frac{\partial^2 \Omega_{\text{MF}}}{\partial \theta^2} \right]^{-1} \cdot \frac{\partial \Omega_{\text{MF}}}{\partial \theta} \Big|_{\theta=\theta_{\text{MF}}} \right)_i \quad (35)$$

(which is Eq. (40) with $f(\theta) = \theta_i$). After some calculation we arrive at the lowest order term in β

$$\begin{aligned} \frac{\partial \Omega}{\partial \theta_i} \Big|_{\theta=\langle \theta \rangle} &= \frac{9}{8} \sum_{jk} \left[\frac{\partial^3 \Omega_{\text{MF}}}{\partial^3 \theta} \right]_{ijk} \left(\left[\frac{\partial^2 \Omega_{\text{MF}}}{\partial \theta^2} \right]^{-1} \cdot \frac{\partial \Omega_{\text{MF}}}{\partial \theta} \right)_j \\ &\quad \left(\left[\frac{\partial^2 \Omega_{\text{MF}}}{\partial \theta^2} \right]^{-1} \cdot \frac{\partial \Omega_{\text{MF}}}{\partial \theta} \right)_k \Big|_{\theta=\theta_{\text{MF}}} \cdots + \text{higher orders}, \end{aligned} \quad (36)$$

which is of order $\beta = 2$, i.e. the self consistency equations are satisfied to the order we have been working in. As a consequence the corrections necessary to account for the fermion sign problem do not modify the mean field equations. A backward reaction on the mean field equations does not occur at this level of the approximation. However we will evaluate further corrections in the course of this work, set forth in Sec. 5, that do have in principle such backward effects on the mean field equation. The present section is focused on evaluating corrections to the effective (Polyakov loop) potential, while section 5 concentrates on the additional effects of pionic and scalar quark-antiquark modes.

Susceptibilities

The formalism allows to determine susceptibilities as well. A susceptibility involving a quantity g can be written in the generic form

$$\chi_g^2 = V \langle (g - \langle g \rangle)^2 \rangle = V \left(\langle g^2 \rangle - \langle g \rangle^2 \right). \quad (37)$$

All that needs to be done is to apply the previously developed formalism to the function g^2 .

In Table 1 the Feynman rules and multiplicity factors are written down for the evaluation of $\langle f \rangle$. In a second step f is replaced by g^2 . In this step attention has to be paid to the prefactors occurring when differentiating g^2 :

$$\begin{aligned} g^2(\theta) \Big|_{\theta=\theta_{\text{MF}}} &= g g \\ \partial_\theta g^2(\theta) \Big|_{\theta=\theta_{\text{MF}}} &= 2g g^{(1)} \\ \partial_\theta^2 g^2(\theta) \Big|_{\theta=\theta_{\text{MF}}} &= 2g g^{(2)} + 2g^{(1)} g^{(1)} \\ \partial_\theta^3 g^2(\theta) \Big|_{\theta=\theta_{\text{MF}}} &= 2g g^{(3)} + 6g^{(1)} g^{(2)} \\ \partial_\theta^4 g^2(\theta) \Big|_{\theta=\theta_{\text{MF}}} &= 2g g^{(4)} + 8g^{(1)} g^{(3)} + 6g^{(2)} g^{(2)}, \end{aligned} \quad (38)$$

where on the right-hand side the argument θ was always suppressed. The superscript (n) denotes the n -th derivative with respect to θ . In this procedure it will happen that vertices of f with $m = 2, 3, \dots$ or more legs will split into two vertices with $m_1 + m_2 = m$ legs

according to Eqs. (38). The lowest orders of the expression, Eq. (37), are shown in Table 2. The contributions of order $(\frac{T}{V})^0$ cancel. In this framework susceptibilities scale with $V^{\frac{1}{2}}$ as expected. Additionally, it may be seen from Table 2 that there are no mean field contributions to susceptibilities in the sense that $\langle (g - \langle g \rangle_{\text{MF}})^2 \rangle_{\text{MF}} = \langle g^2 \rangle_{\text{MF}} - \langle g \rangle_{\text{MF}}^2 = g_{\text{MF}}^2 - g_{\text{MF}}^2 = 0$.

Interpretation of the Feynman diagrams

The first diagram in the upper line of Eq. (28) can be interpreted as an insertion modelling vacuum excitations. When explicitly applying the described formalism to the PNJL model one finds that δ has significant contributions only from the field ϕ_8 (recall that $\phi_8 = 0$ in the mean field limit). This term allows the absorption and emission of gluonic quanta, associated with ϕ_8 , out of the vacuum. In general, this term is also present in the case where the quark chemical potential μ is zero. In this case the emission and absorption processes exactly cancel. As soon as $\mu \neq 0$ this balance is disturbed. The residual imaginary gradient acts as a source (sink) term for the fields. In the present PNJL context it is only the quasi-gluon field ϕ_8 that shows such a non-vanishing source term.

Comparison with the saddle point approximation

In the saddle point approximation the integration over the real fields from minus to plus infinity is treated as a contour integral in the complex plane. If the integrand (which here is the exponential of the action e^{-S_E}) is analytic in the complex plane the contour of integration may in general be deformed as long as the endpoints (here: $-\infty \in \mathbb{R}$ and $+\infty \in \mathbb{R}$) remain fixed. For an approximation of such a contour integral it is helpful to choose a path which keeps the complex phase of the integrand fixed. This can be achieved by choosing the path of steepest descent. The saddle point method approximates the value of the integral by the maximal value of the integrand on the contour of steepest descent. This extremal point is a saddle point. The necessary condition for a saddle point is a vanishing first derivative of the action with respect to the fields. This is the requirement of Eq. (16) which now has to be understood as a set of complex equations with the solutions θ_{saddle} . In general the solution to these equations requires that all fields assume complex values. The action, now interpreted as a complex function, has a physical interpretation when evaluated at the saddle point $\theta = \theta_{\text{saddle}}$.

The saddle point approximation is applicable if the integrand may be cast into the form of an exponential $e^{f(x)}$ where $f(x)$ is analytic on the whole region of integration and its continuation required for the deformation of the integration path. The integral $\int d\theta g(\theta) e^{-S_E}$ needed for the evaluation of a thermodynamic expectation value of a quantity $g(\theta)$ can be rewritten as $\int d\theta e^{-S_E + \log(g(\theta))}$. Here the saddle point approximation is applicable only if $g(\theta)$ does not have any zeros in the region of integration and its analytic continuation. For the Polyakov loop Φ and its complex conjugate Φ^* (interpreted as functions of ϕ_3 and ϕ_8 , i. e. $\Phi = \Phi(\phi_3, \phi_8)$ and $\Phi^* = \Phi^*(\phi_3, \phi_8)$) the periodic region of integration in the ϕ_3 - ϕ_8 -plane may be chosen such that all zeros of Φ and Φ^* lie on boundaries of the region of integration. For the chiral field σ , the diquark field Δ and the field ϕ_3 no deformation of the integration path needs to be performed: the path of steepest descent is the original path of integration along the real axis. In this case the application of the saddle point approximation is trivial and produces the correct values for the approximation of the thermal expectation values $\langle \sigma \rangle$, $\langle \Delta \rangle$ and $\langle \phi_3 \rangle$. In the case of ϕ_8

Table 1: The Feynman graphs contributing to $\langle f \rangle$, ordered in $(\frac{T}{V})^\alpha$ and δ^β with multiplicity factors.

Table 2: The lowest order Feynman graphs contributing to χ_g^2 as defined in Eq. (37). The vertices depicted as a circle are now the contributions of g , defined analogously to the contributions of f in Eq. (34). The prefactors are the product of the multiplicity factors of the original Feynman graphs and the factors arising from the differentiation, Eq. (38).

the path would need to be deformed, however. As ϕ_8 is zero within the deformation region of the path and $\log(\phi_8)$ is non-analytic, the saddle point approximation cannot produce a meaningful approximation of $\langle \phi_8 \rangle$.

The saddle point method, when used to approximate path integrals determining the partition function and thermal expectation values, may transfer certain fluctuations into shifted mean fields, concealing the origin of such fluctuations. This is implicit in the procedures applied in Refs. [14, 16–19] where both $\langle \Phi \rangle$ and $\langle \Phi^* \rangle$ were treated as *independent* degrees of freedom. The translation back into the gauge fields $A_3 = T\phi_3$ and $A_8 = T\phi_8$ can then no longer be performed on the basis of Eqns. (3, 4).

Approximating the mean field effective action Ω_{MF} by its Taylor series about the solution of Eq. (17) we can solve Eq. (16) resulting in a shift of the fields, which is given to lowest order by Eq. (35). Of course also higher orders can be evaluated, giving additional corrections to θ_{MF} . Substituting Eq. (35) back into Ω_{MF} as a function of θ gives the result found previously. As the saddle point approximation comprises the limit $\frac{V}{T} \rightarrow \infty$ only the leading order results in the thermodynamic expansion can be reproduced.¹² For susceptibilities the saddle point approximation will always produce a vanishing result.¹³

Closing this brief lineup of saddle point approximation and the approach via the integration of fluctuations presented here, one concludes the equivalence of both methods in the thermodynamic limit $\frac{V}{T} \rightarrow \infty$ for entities that satisfy all preconditions for the saddle point approximation. Fluctuations however cannot be traced systematically in the saddle point approximation. Quantities involving cancellations in the thermodynamic limit, such as susceptibilities, are not accessible in the saddle point approximation. In particular, the second derivative of the action at the saddle point is not directly related to the susceptibilities by a simple matrix inversion. In this sense the present approach is more general and more versatile in its applications, while the saddle point method is technically less involved.

4 Results

The numerical calculations presented in this section were performed in the thermodynamic limit, i. e. in leading order of the $\frac{T}{V}$ -expansion, and up to first order in the δ -expansion. The thermodynamic potential is then determined by¹⁴

$$\Omega = \Omega_{\text{MF}} - \frac{1}{2} \frac{T}{V} \text{---}\times\text{---} = \Omega_{\text{MF}} - \frac{1}{2} \left(\frac{\partial \Omega_{\text{MF}}}{\partial \theta} \right)^T \cdot \left[\frac{\partial^2 \Omega_{\text{MF}}}{\partial \theta^2} \right]^{-1} \cdot \frac{\partial \Omega_{\text{MF}}}{\partial \theta} \Big|_{\theta=\theta_{\text{MF}}}, \quad (39)$$

where Ω_{MF} has been calculated in [20]. Thermal expectation values are then computed as follows

$$\langle f \rangle = f(\theta_{\text{MF}}) + \text{---}\circ\text{---} = f(\theta_{\text{MF}}) - \left(\frac{\partial \Omega_{\text{MF}}}{\partial \theta} \right)^T \cdot \left[\frac{\partial^2 \Omega_{\text{MF}}}{\partial \theta^2} \right]^{-1} \cdot \frac{\partial f}{\partial \theta} \Big|_{\theta=\theta_{\text{MF}}}. \quad (40)$$

¹²In the limit $\frac{V}{T} \rightarrow \infty$ higher order corrections originating in the (perturbative) part of the action \mathcal{S}_1 are reproduced correctly as well, once the shift of the mean fields $\delta\vec{\theta}$ includes these higher order corrections.

¹³The square of the susceptibility of the quantity g is defined proportional to $\langle \Delta g \rangle^2 = \langle (g - \langle g \rangle)^2 \rangle = (g(\theta_{\text{saddle}}) - g(\theta_{\text{saddle}}))^2 = 0$.

¹⁴Note that a Feynman graph for a correction is used here to express the lowest order correction to the thermodynamic potential. This term however still belongs to the contributions of the unperturbed action $\mathcal{S}_{\text{Gauss}}(k)$ given in Eq. (24).

The difficulty in evaluating higher order diagrams originates in the finite precision of numerical differentiation, which is at the centre of the evaluation of all vertices and propagators. Numerical instabilities can easily produce uncertainties that are larger than the correction itself.

4.1 The Polyakov loop $\langle\Phi\rangle$ and its conjugate $\langle\Phi^*\rangle$

For the Polyakov loop $\langle\Phi\rangle$ and its conjugate $\langle\Phi^*\rangle$ when treated as described in the previous section, the mean field analysis determines them to be equal. The corrections to mean field split the values of $\langle\Phi\rangle$ and $\langle\Phi^*\rangle$: it is the fluctuations of the homogeneous gluonic fields that cause this split.

The difference $\langle\Phi^*\rangle - \langle\Phi\rangle$ vanishes at zero quark chemical potential μ and has the same sign as μ . As can be seen from Fig. 3 the difference $\langle\Phi^*\rangle - \langle\Phi\rangle$ is large around the phase transitions. In the upper left panel of Fig. 3 the influence of the first order phase transition separating the chiral and the diquark phase at low temperature can be seen as a jump in both $\langle\Phi\rangle$ and $\langle\Phi^*\rangle$. The second order phase transition separating the diquark regime from the high temperature quark-gluon phase can be identified as a kink in the lower right panel of Fig. 3.

4.2 Phase diagram

Using the calculated susceptibilities one can now draw a phase diagram in the plane of temperature and chemical potential. There are several ways to determine the cross-over transition line separating the phase of spontaneously broken chiral symmetry from the quark gluon plasma phase. In Fig. 4 two such criteria are compared: the maximum in the chiral susceptibility χ_M or Polyakov loop susceptibility $\chi_{\text{Re}\Phi}$ and the maximal change of the constituent quark mass or the Polyakov loop, both signalise the rapid cross-over transition. The susceptibilities are defined by Eq. (37) and can be expressed in terms of the inverse matrix of the second derivative of the full thermodynamic potential:

$$\chi_M^2 = V \left(\langle m^2 \rangle - \langle m \rangle^2 \right) = T \left[\frac{\partial^2 \Omega_{\text{full}}}{\partial \theta_i \partial \theta_j} \right]_{m, m}^{-1} \quad (41)$$

$$\chi_\Phi^2 = V \left(\langle \Phi^2 \rangle - \langle \Phi \rangle^2 \right) = T \left[\frac{\partial^2 \Omega_{\text{full}}}{\partial \theta_i \partial \theta_j} \right]_{\Phi, \Phi}^{-1} \quad (42)$$

$$\chi_{\text{Re}\Phi}^2 = \frac{T}{4} \left[\frac{\partial^2 \Omega_{\text{full}}}{\partial \theta_i \partial \theta_j} \right]_{\Phi, \Phi}^{-1} + \frac{T}{2} \left[\frac{\partial^2 \Omega_{\text{full}}}{\partial \theta_i \partial \theta_j} \right]_{\Phi, \Phi^*}^{-1} + \frac{T}{4} \left[\frac{\partial^2 \Omega_{\text{full}}}{\partial \theta_i \partial \theta_j} \right]_{\Phi^*, \Phi^*}^{-1}. \quad (43)$$

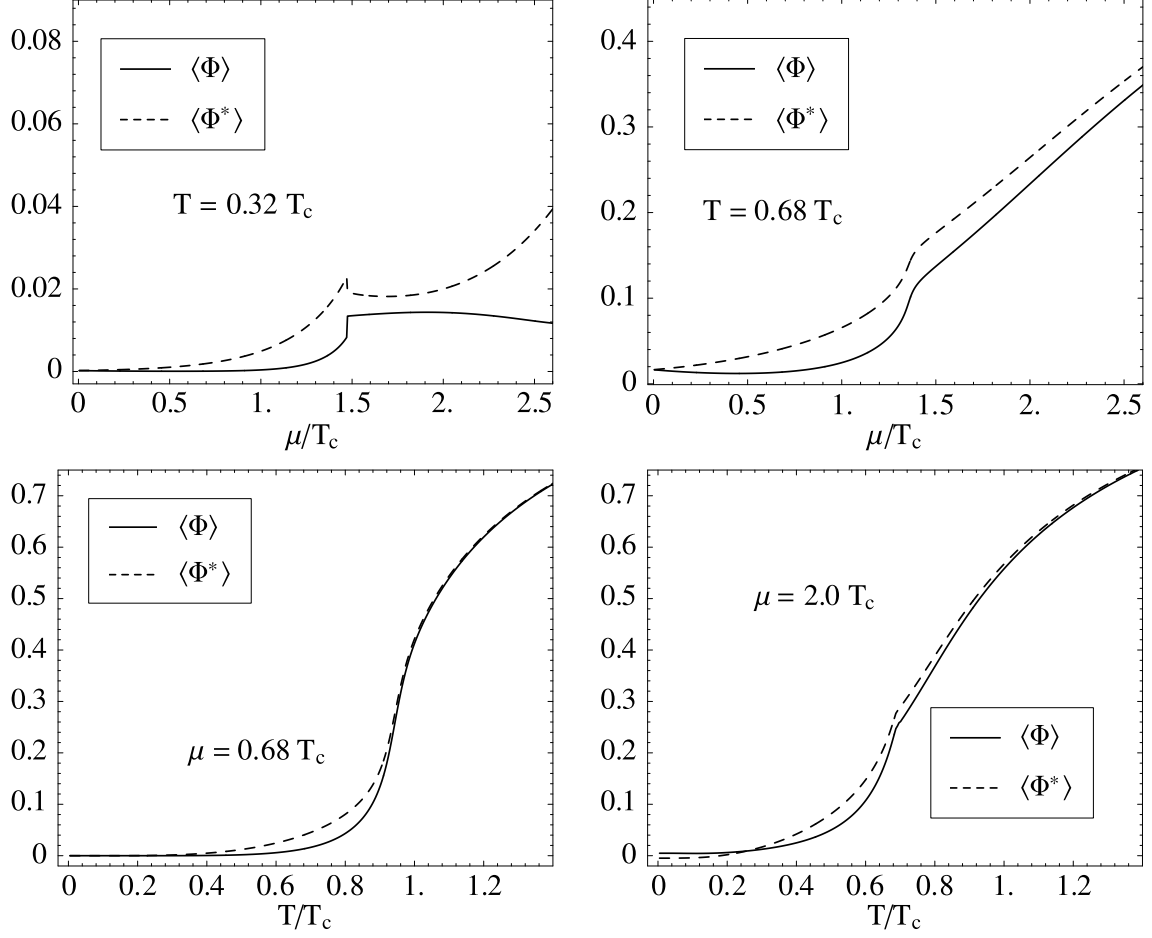


Figure 3: Examples of thermal expectation values of the Polyakov loop $\langle\Phi\rangle$ and its conjugate $\langle\Phi^*\rangle$. In the upper row $\langle\Phi\rangle$ and $\langle\Phi^*\rangle$ are plotted as functions of the chemical potential μ at constant temperature T . Below $\langle\Phi\rangle$ and $\langle\Phi^*\rangle$ are plotted as functions of temperature T at constant chemical potential μ .

These susceptibilities are calculated using the graphs shown in Tab. 2 which translate into the explicit form:

$$\begin{aligned}
\chi^2 = & T \left(\frac{\partial g}{\partial \theta} \right)^T \cdot \left[\frac{\partial^2 \Omega_{\text{MF}}}{\partial \theta^2} \right]^{-1} \cdot \frac{\partial g}{\partial \theta} \Big|_{\theta=\theta_{\text{MF}}} \\
& - 2 T \left(\frac{\partial g}{\partial \theta} \right)^T \cdot \left[\frac{\partial^2 \Omega_{\text{MF}}}{\partial \theta^2} \right]^{-1} \cdot \frac{\partial^2 g}{\partial \theta^2} \cdot \left[\frac{\partial^2 \Omega_{\text{MF}}}{\partial \theta^2} \right]^{-1} \cdot \frac{\partial \Omega_{\text{MF}}}{\partial \theta} \Big|_{\theta=\theta_{\text{MF}}} \\
& + T \sum_{i,j,k} \frac{\partial^3 \Omega_{\text{MF}}}{\partial \theta_i \partial \theta_j \partial \theta_k} \left(\left[\frac{\partial^2 \Omega_{\text{MF}}}{\partial \theta^2} \right]^{-1} \cdot \frac{\partial g}{\partial \theta} \right)_i \left(\left[\frac{\partial^2 \Omega_{\text{MF}}}{\partial \theta^2} \right]^{-1} \cdot \frac{\partial g}{\partial \theta} \right)_j \\
& \times \left(\left[\frac{\partial^2 \Omega_{\text{MF}}}{\partial \theta^2} \right]^{-1} \cdot \frac{\partial \Omega_{\text{MF}}}{\partial \theta} \right)_k \Big|_{\theta=\theta_{\text{MF}}} + O(\beta = 2) + O(\alpha = 2) \quad (44)
\end{aligned}$$

Here g is to be substituted by m or $\text{Re } \Phi$, respectively. The first term in Eq. (44) is the susceptibility of the Gaussian theory whereas the other terms are interpreted as corrections. As both criteria are linked via the quadratic term in the action, all curves finally converge to the same point, the critical point in the absence of diquark condensation. A singularity in the second derivative of the action (or equivalently in the propagator) enforces this unique intersection point, where the specific heat and other quantities show singular behaviour.

In Fig. 5 we show the chiral and the Polyakov loop susceptibilities as functions of temperature at vanishing quark chemical potential (left panel) and compare them to the temperature derivatives of the constituent quark mass and the Polyakov loop (right panel). If we consider the behaviour of χ_M , $\chi_{\text{Re } \Phi}$ and χ_Φ at $T \rightarrow 0$ we find that $\chi_{\text{Re } \Phi}$ is finite, while χ_M and χ_Φ vanish. This can be explained by the fact that $(\text{Re } \Phi)^2 = \frac{1}{4}(\Phi^2 + 2|\Phi|^2 + \Phi^{*2})$ has a U(1)-symmetric term $|\Phi|$. As the U(1) symmetry incorporates the $Z(3)$ centre of $\text{SU}(3)_c$ this term does not have to vanish once the $Z(3)$ symmetry is fully restored at $T = 0$.¹⁵ The width of the peak in the temperature derivative of the constituent quark mass $m = m_0 - \sigma$ suggests that this cross-over is influenced by the cross-over of the Polyakov loop. At finite current quark mass m_0 the PNJL model produces an approximate coincidence of the peaks in the susceptibilities of the Polyakov loop and the constituent quark mass m .

A comparison of the phase diagram obtained in mean field approximation in Ref. [20] and the phase diagram including corrections to the order $\beta \leq 1$ shown in Fig. 6, explicitly approves that corrections to the phase diagram due to fluctuations are small [20].

4.3 Moments of the pressure

One benchmark for the PNJL model is its surprising capability of reproducing the trends of lattice QCD calculations.¹⁶ One way to handle the fermion sign problem in lattice QCD is to expand the calculated pressure about $\mu = 0$. Such an expansion is given in Ref. [8]:

$$\frac{p(T, \mu)}{T^4} = \sum_{n=0}^{\infty} c_n(T) \left(\frac{\mu}{T} \right)^n \quad \text{with} \quad c_n(T) = \frac{1}{n!} \frac{\partial^n (p(T, \mu)/T^4)}{\partial (\mu/T)^n} \Big|_{\mu=0} \quad (45)$$

¹⁵The authors thank Chihiro Sasaki for pointing this out to them.

¹⁶Note however the discussion concerning the dependence on quark masses in Ref. [26].

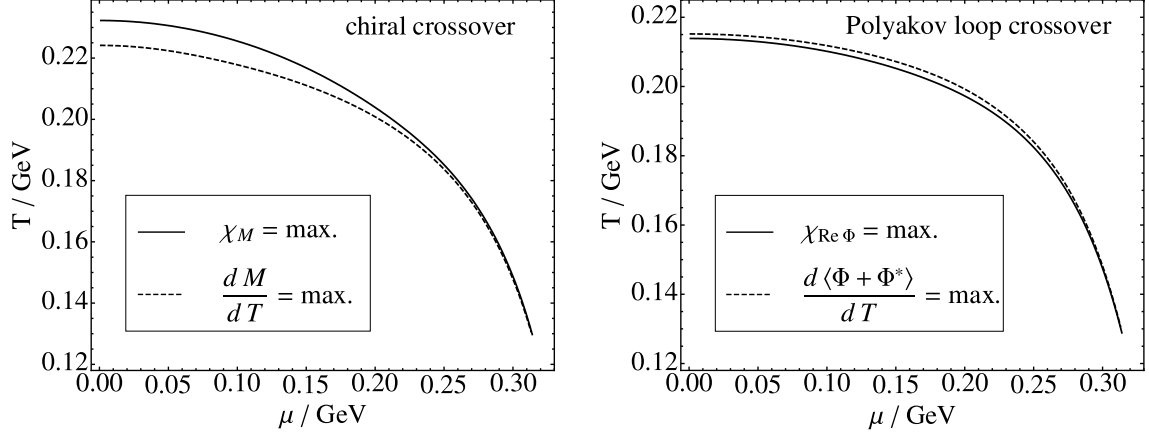


Figure 4: Comparison of the transition lines obtained by determination of the maximum in the chiral susceptibility (left panel solid line) and the Polyakov loop susceptibility $\chi_{\text{Re } \Phi}$ (right panel solid line) with the transition lines fixed by the maximal change with respect to temperature of constituent quark mass (left panel dashed line) and average of the real part of the Polyakov loop $\frac{1}{2} \langle \Phi + \Phi^* \rangle$ (right panel dashed line).

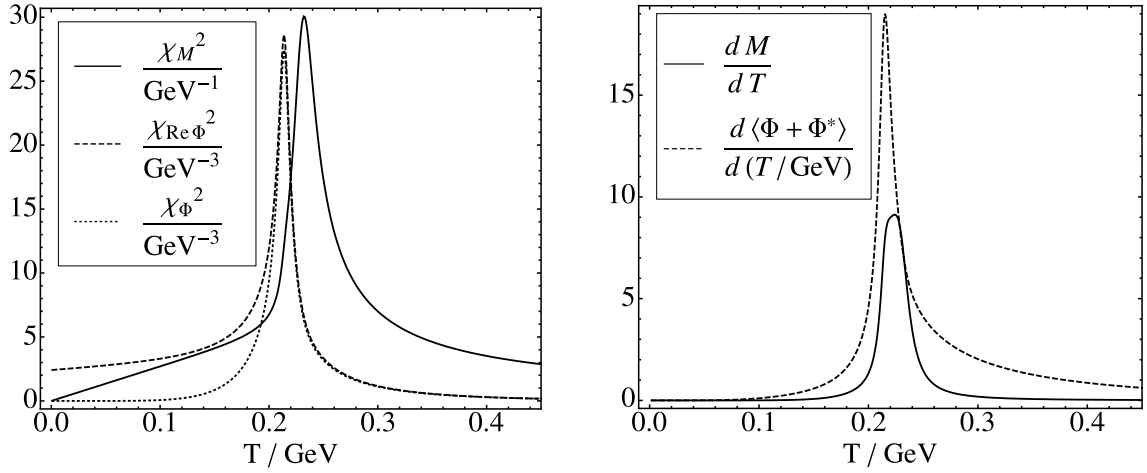


Figure 5: The chiral susceptibility χ_M (left panel solid line) and the Polyakov loop susceptibilities $\chi_{\text{Re } \Phi}$ (left panel dashed line) and χ_Φ (left panel dotted line) plotted as functions of temperature at vanishing quark chemical potential. These susceptibilities defined by Eqs. (41, 42, 43) and evaluated using Eq. (44) are compared here to the derivative of the constituent quark mass (right panel solid line) and the expectation value of the real part of the Polyakov loop (right panel dashed line) with respect to temperature.

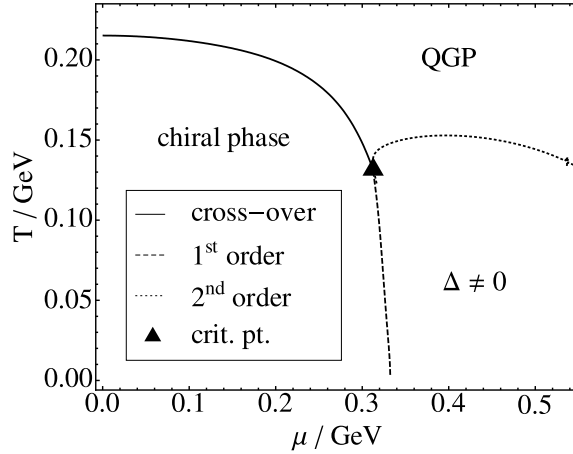


Figure 6: Phase diagram implementing corrections to the order $\beta \leq 1$. Solid lines: cross-over transition of the susceptibility related to the real part of the Polyakov loop, dashed lines: first order phase transition, and dotted: second order phase transitions.

with even n as the situation is charge conjugation invariant. Specifically:

$$\begin{aligned}
 c_2 &= \frac{1}{2} \frac{\partial^2(p/T^4)}{\partial(\mu/T)^2} \Big|_{\mu=0}, & c_4 &= \frac{1}{24} \frac{\partial^4(p/T^4)}{\partial(\mu/T)^4} \Big|_{\mu=0}, \\
 c_6 &= \frac{1}{720} \frac{\partial^6(p/T^4)}{\partial(\mu/T)^6} \Big|_{\mu=0}, & c_8 &= \frac{1}{40320} \frac{\partial^8(p/T^4)}{\partial(\mu/T)^8} \Big|_{\mu=0}.
 \end{aligned} \tag{46}$$

The pressure in the PNJL model is evaluated by subtracting the divergent vacuum contributions

$$p = \Omega - \Omega(T=0) \tag{47}$$

Only the lowest order correction ($(T/V)^0$ and δ^1) is used for the evaluation of the c_n illustrated in Fig. 7. In comparison with the plots for c_n shown in a previous paper [20] at the mean field level the moments c_n show slightly more structure. The rise in c_2 is somewhat sharper, the peak in c_4 is about 5% higher. In summary, however, the corrections induced so far by fluctuations around the mean fields are small. Pionic fluctuations, to be discussed in Sec. 5, tend to be more important. In presently available lattice results [8], these effects are however suppressed by the relatively large pion masses.

4.4 Speed of sound

In Fig. 8 the squared speed of sound in units of the speed of light is plotted as a solid line. The speed of sound v_s is defined by

$$v_s^2 = \frac{\partial p}{\partial \varepsilon} \Big|_S = \frac{\partial \Omega}{\partial T} \Big|_V \Big/ T \frac{\partial^2 \Omega}{\partial T^2} \Big|_V, \tag{48}$$

where the denominator is the specific heat capacity c_V . The dashed line in Fig. 8 gives the size of the ratio of pressure and energy density, $\frac{p}{\varepsilon}$. In the panel to the left where the quantities are plotted at vanishing chemical potential $\mu = 0$ both graphs show a pronounced dip near the crossover transition temperature. In the panel to the right the same situation is plotted at a quark chemical potential close to the chemical potential of the critical point $\mu \lesssim \mu_{\text{crit.}}$

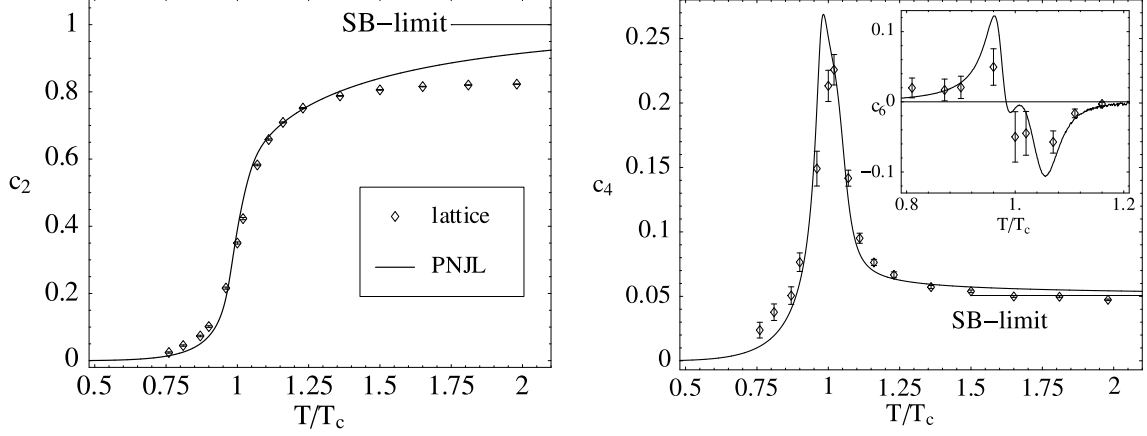


Figure 7: The moments of the pressure with respect to $\frac{\mu}{T}$ as defined in Eq. (45). c_2 is shown in the left panel, c_4 is displayed to the right where c_6 is shown in the inset. The data deduced from lattice computations are taken from [8].

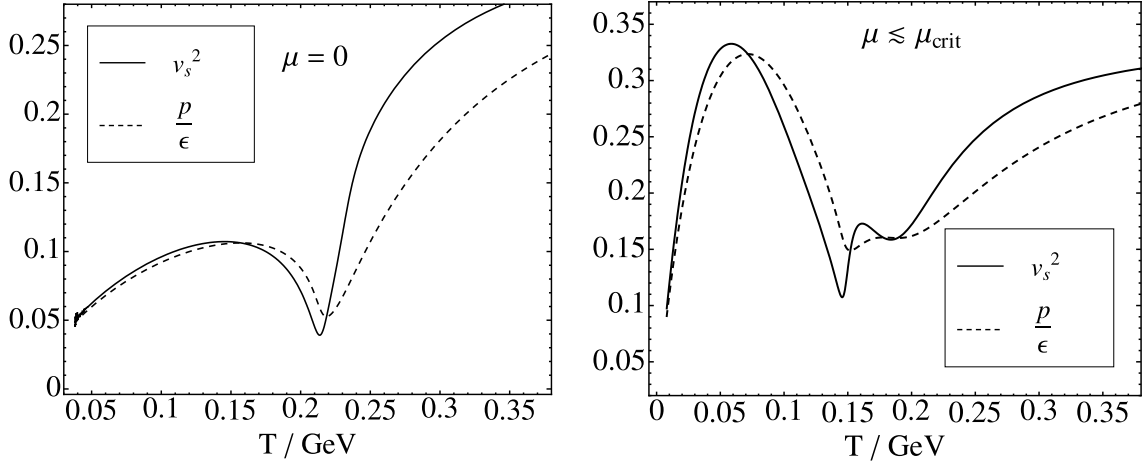


Figure 8: The speed of sound (solid) and the ratio of pressure over energy density (dashed) at vanishing chemical potential as function of temperature (left panel). The right panel shows the same quantities at a quark chemical potential slightly less than the one at the critical point ($\mu = 0.3 \text{ GeV} \lesssim \mu_{\text{crit}} \simeq 0.31 \text{ GeV}$).

5 Dynamical fluctuations

So far the formalism presented has been focused on the treatment of fluctuations around the mean fields, averaged over space and (Euclidean) time. The homogeneous, constant Polyakov loop field and its corrections beyond mean field fall in this category.

In this section we consider mesonic excitations and their propagation (i.e. $\frac{1}{N_c}$ -corrections). The NJL framework is well suited to incorporate such effects. The NJL model features a dynamical mechanism which produces spontaneous chiral symmetry breaking and, at the same time, generates the pion as a Goldstone boson in the pseudoscalar quark-antiquark channel, together with a massive scalar (sigma) boson. The thermodynamics of these modes and their changing spectral properties have been subject of several NJL model calculations in the past [27–29].

With increasing temperature, the mass of the pion is still protected by its Goldstone boson nature, whereas the sigma mass drops until at $T \sim T_c$ it becomes degenerate with the pion, signalling restoration of chiral symmetry in its Wigner-Weyl realization. For $T > T_c$, the π and σ masses jointly increase quite rapidly while at the same time their widths for decay into $q\bar{q}$ grow continuously. This implies that at temperatures exceeding T_c both π and σ modes become thermodynamically irrelevant while correlated quark-antiquark pairs carrying the quantum numbers of π and σ can still be active above T_c . One therefore expects that the corrections to the pressure from propagating pions and sigmas should be concentrated around T_c . These mesonic modes are colour singlets¹⁷. Thus their statistical weight is much smaller than the weight of the deconfined quark quasiparticles.

5.1 Derivation of meson propagators from the PNJL model

We start from the derivation of mesonic propagators in the PNJL model as performed, for example, in [30]. We generalise Eq. (28), where the momentum argument of the fields is suppressed as it has been implied that $\xi = \xi(q^\mu = 0)$. We release this limitation and calculate the momentum dependent propagator

$$\frac{j \xrightarrow{q^\mu} k}{=} = \left[\frac{\partial^2 \mathcal{S}_{\text{bos}}}{\partial \xi_j(q^\mu) \partial \xi_k(-q^\mu)} \right]^{-1}, \quad (49)$$

where ξ now stands for the pion or sigma fields. Note that the functional trace in the formula for \mathcal{S}_{bos} ensures momentum conservation, such that the sum of the momentum arguments in the denominator always vanishes. The calculation can be done numerically as it was done in the previous section. Alternatively, we use an analytic approach as follows. Recall some useful formulae also exploited in Refs. [6, 8]:

$$\frac{\partial \ln \det M}{\partial x} = \text{tr} \left[M^{-1} \frac{\partial M}{\partial x} \right] \quad \text{and} \quad \frac{\partial M^{-1}}{\partial x} = -M^{-1} \frac{\partial M}{\partial x} M^{-1}, \quad (50)$$

with M an invertible matrix and $\frac{\partial M}{\partial x}$ is the component-wise derivative of this matrix. Applying this to the PNJL action \mathcal{S}_{bos} in (9) and neglecting the potential terms for the

¹⁷Colour octet quark-antiquark modes turn out to be heavy and far removed from the spectrum of active degrees of freedom.

moment we find

$$\frac{\partial \mathcal{S}_{\text{bos}}}{\partial \theta} = -\frac{V}{2} \sum_n \int \frac{d^3 p}{(2\pi)^3} \text{Tr} \left[\tilde{S}(i\omega_n, \vec{p}; \theta) \frac{\partial \tilde{S}^{-1}(i\omega_n, \vec{p}; \theta)}{\partial \theta} \right], \quad (51)$$

where $\tilde{S}^{-1}(i\omega_n, \vec{p}; \theta)$ denotes the inverse quark propagator with emphasis on the fact that the quark propagates in the mesonic background field θ . This formalism makes it possible to calculate derivatives with respect to bosonic fields (say θ_k) that have not been explicitly included in the action, as long as it is ensured that the model does not produce finite vacuum expectation values for these particular fields. Not having a vacuum expectation value is equivalent to the fact, that the mean field equations corresponding to these fields are satisfied for a vanishing field, i. e. that

$$\left. \frac{\partial \mathcal{S}_{\text{bos}}}{\partial \theta} \right|_{\theta_k=0} = 0. \quad (52)$$

All we need to know is the constant matrix $\frac{\partial \tilde{S}^{-1}}{\partial \theta_k}$. This matrix involves the Dirac, colour and flavour structure of a quark-antiquark pair (or a quark-quark pair) that couples to the bosonic field θ_k , i. e. it is determined by the quantum numbers of θ_k . The mean field equation is fulfilled if the trace in Eq. (51) vanishes for the given Dirac, colour and flavour structure. For the pion field this is true as long as there is no pion condensate.¹⁸ The condensate corresponding to the sigma, namely the chiral condensate, figures explicitly in the action and is therefore included in the quark propagator.

In the case of the pion and sigma propagators the functional derivative in (49) produces exactly the trace over Dirac, colour and flavour structures known from RPA calculations [27–30]. We adopt the definition of the quark distribution functions f_{Φ}^+ and f_{Φ}^- and the separation of the emerging integral into the contributions I_1 and I_2 as given in Ref. [30]. In the treatment of the thermodynamics we have modified the cutoff prescription of the standard NJL model, such that non-divergent integrals are integrated over the whole quark-momentum range, while only divergent integrals are regularised by the usual NJL three-momentum cutoff. The separation of finite and divergent contributions is defined such that the model reproduces the classical limit at high temperatures, i. e. the Stefan-Boltzmann limit. As a downside, for consistency all newly appearing integrals have to be treated in the same manner, which leads to slightly different results from those given in Ref. [30].

5.2 Mesonic corrections to the pressure

Once the meson propagators are given, it is possible to evaluate the contribution to the pressure from mesons propagating in the heat bath using RPA methods. Applying Bethe-Salpeter (RPA) equations generates spectral functions

$$\rho_{\text{M}}(\omega, \vec{q}; T) = \frac{G \text{Im} \Pi_{\text{M}}(\omega, \vec{q}; T)}{(1 - G \text{Re} \Pi_{\text{M}})^2 + (G \text{Im} \Pi_{\text{M}})^2}$$

with the thermal quark-antiquark polarization function

$$\Pi_{\text{M}}(\omega, \vec{q}; T) = T \sum_{\omega_n} \int \frac{d^3 p}{(2\pi)^3} \text{Tr} \left[\Gamma_{\text{M}} \tilde{S}(i\omega_n + \mu, \vec{p}) \Gamma_{\text{M}} \tilde{S}(i(\omega_n - \omega) + \mu, \vec{p} - \vec{q}) \right],$$

¹⁸The mean field equation is satisfied as the flavour-trace $\text{tr}_f[\mathbb{1} \tau_i] = 0$ with $i = 1, 2, 3$ vanishes.

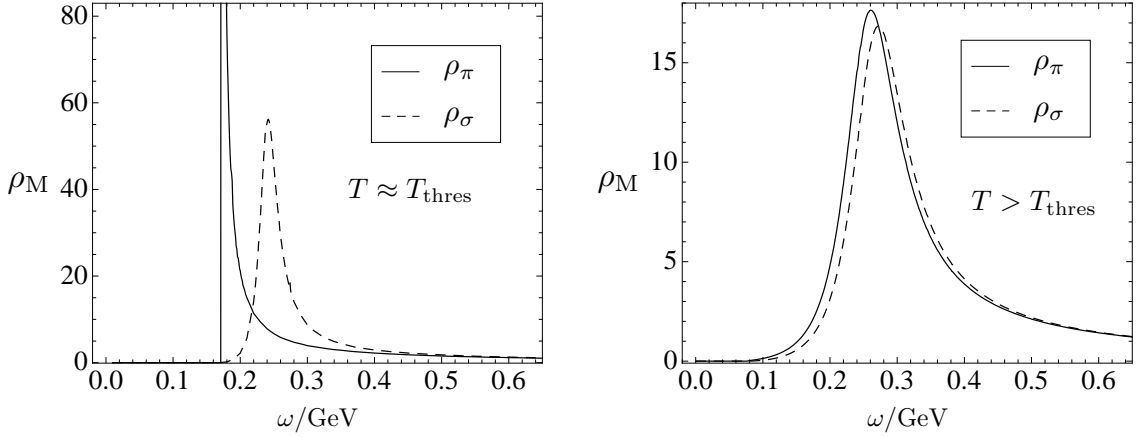


Figure 9: The spectral functions $\rho_M = \frac{G \text{Im} \Pi_M}{(1 - G \text{Re} \Pi_M)^2 + (G \text{Im} \Pi_M)^2}$ taken at $\vec{q} = 0$ for pion and sigma at $T \approx T_{\text{thres}}$ (left) and at $T > T_{\text{thres}}$ (right).

where the sum is taken over the Matsubara frequencies $\omega_n = (2n + 1)\pi T$. Here Γ_M is a Dirac, flavour and colour representation of a meson current labelled M. In this work we only focus on the pseudoscalar isovector channel (i.e. pionic excitations) and the scalar isoscalar channel. $\tilde{S}(i\omega_n, \vec{p}) = -\frac{m + \not{p}}{\omega_n^2 + p^2 + m^2}$ denotes the quark quasiparticle propagator with $\not{p} = i\omega_n \gamma_0 - \vec{\gamma} \cdot \vec{p}$.

The pressure below T_c is essentially generated by the pion pole with its almost temperature independent position. Therefore the calculated pressure below T_c basically represents the one of a pion gas with fixed (temperature independent) mass. Fig. 9 shows, as examples, the spectral functions for the pion and sigma modes at threshold temperature where the breakup into a quark-antiquark pair occurs. At this point the π and σ spectral functions are still distinguishable (left panel of Fig. 9), whereas they coincide (right panel) at temperatures well above threshold where π - σ degeneracy indicates restoration of chiral symmetry in its Wigner-Weyl realization. Their width is a measure of the decay of the (increasingly massive) pionic and sigma modes into (light) deconfined quark-antiquark pairs at temperatures above T_c .

The resonant interaction of unstable mesons with the quark sea above T_c produces an additional pressure contribution. This contribution is not part of the quark pressure previously calculated in Hartree-Fock approximation. The meson decay products form rings of RPA chains. Such kind of pressure contributions are investigated in Ref. [31] and calculated performing the ring sum. However, below T_c the NJL model does not handle the mesonic degrees of freedom properly. In the hadronic phase the coupling of mesonic modes to the quark-antiquark continuum is suppressed by confinement, whereas ρ_M receives contributions from decays into $q\bar{q}$ even below T_c . This unphysical feature persists [30] in the PNJL generalisation of the NJL approach. Moreover, the non-renormalizability of the NJL model requires to introduce further subtractions when following the lines of Ref. [31]. To avoid such arbitrariness and unphysical features we ignore the decay of meson modes into $q\bar{q}$ -pairs altogether when calculating an estimate for the meson contributions to the pressure:

$$\delta\Omega = \nu \int \frac{d^3q}{(2\pi)^3} T \ln(1 - e^{-E_q/T}) + B(T) , \quad (53)$$

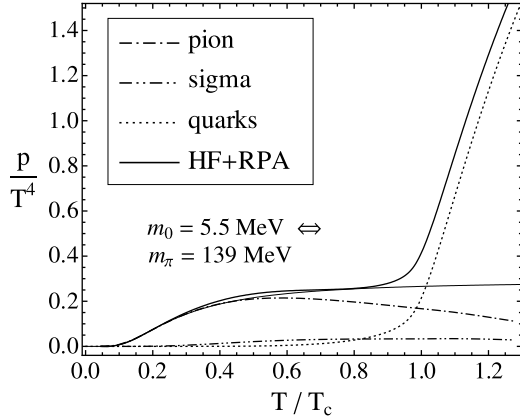


Figure 10: The pressure contribution originating from pion modes, sigma modes and from quarks in Hartree-Fock approximation (dotted). The thin solid line represents the pressure of a gas of bosons with three internal degrees of freedom and a constant mass $m = m_\pi(T = 0)$.

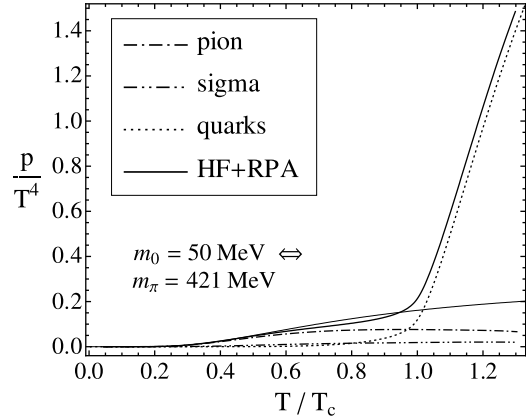


Figure 11: Same as Fig. 10, but with higher current quark mass $m_0 = 50 \text{ MeV} \Rightarrow m_\pi = 421 \text{ MeV}$ (compared to $m_0 = 5.5 \text{ MeV} \Rightarrow m_\pi = 139 \text{ MeV}$ in Fig. 10). The pressure of the boson gas (thin solid line) was now plotted using the heavier pion mass.

where ν is the statistical weight of the corresponding meson species, $E_q = \sqrt{\vec{q}^2 + m_{\text{pole}}^2(T)}$ with $m_{\text{pole}}(T)$ the temperature dependent pion and sigma pole mass determined by $1 - G \text{Re} \Pi = 0$. Furthermore $B(T)$ is an appropriately chosen vacuum energy constant ensuring thermodynamic consistency. $B(T)$ is fixed such that the temperature dependence of the pole mass $m_{\text{pole}}(T)$ is compensated on differentiating Ω with respect to the temperature T . This implies that the inclusion of $B(T)$ ensures that $\partial\Omega/\partial m_{\text{pole}}|_T = 0$.

In Fig. 10 the calculated pressure of $\pi^{0,\pm}$ and sigma modes are compared with the quark Hartree-Fock pressure and the result for the overall pressure of Hartree-Fock plus RPA is plotted. For comparison the pressure of a Bose gas with three internal degrees of freedom is indicated by the thin solid line. Below the cross-over temperature T_c one can clearly identify the pion gas contribution resulting from the RPA calculations. Once the meson masses reach the scale of the NJL cutoff Λ the used approximation breaks down. The inversion of the scale hierarchy appears at temperatures of about $1.3 T_c$. For larger current quark masses the meson gas contributions and correlations are reduced. This effect is illustrated by Fig. 11 where the pressure of the PNJL model is plotted using an increased current quark mass leading to an unphysically heavy pion. Thus for heavy pions the agreement with lattice data observed in a previous publication [20] remains. This agreement is also confirmed by calculations in a non-local PNJL framework [32] which does not suffer from cutoff artefacts.

6 Conclusions and outlook

The PNJL model as a model for QCD thermodynamics picks up on two known properties of QCD: spontaneous chiral symmetry breaking and confinement. In this work some of the existing calculations [14, 20, 21] have been extended. We have reviewed the expectation values of the Polyakov loop and its complex conjugate, the phase diagram, the moments of

the pressure and the speed of sound in a framework beyond mean field theory. While the phase diagram does not show significant changes when improving the mean field approximation, the moments of the pressure and the speed of sound show quantitative differences on the order of 5 %. In general the structures observed become more articulate. In the case of the Polyakov loop and its complex conjugate the corrections cause qualitative differences. While the Polyakov loop and its complex conjugate are equal at mean field level in the present approach, the corrections to the mean field result generate the split of the two expectation values $\langle\Phi\rangle$ and $\langle\Phi^*\rangle$ at non-zero quark chemical potential.

The extensions beyond mean field are based on a perturbative method, resulting in systematically ordered series of corrections. This perturbative expansion can also treat the imaginary parts of the action properly: up to the order of approximation the constructed effective action is a real valued function and, additionally, the expectation values of real quantities are real numbers. Therefore, the presented formalism is a systematic way to treat the fermion sign problem in the PNJL model. As all perturbative approaches, this method relies on the existence of a unique ground state around which all field configurations with an action close to the minimal action are concentrated. This ensures that an expansion about this ground state is a meaningful approximation. It is the choice of the proper degrees of freedom that is the precondition for the practicability of this approximation. For a unique ground state the size of the corrections hints on how close to the true minimum the expansion point is located. One of the strengths of this procedure is that the zeroth order of the perturbative expansion is the mean field result and, therefore, already incorporates spontaneous chiral symmetry breaking and its temperature dependence.

The presented calculations suggest that the presence of the fermion sign problem enhances the discrepancies between classical and quantum mechanical results. The numerical results show that the corrections are largest in the vicinity of phase transitions or rapid cross-overs. This comes as no surprise as it is the transitional region between two states where we expect large fluctuations.

The degrees of freedom that govern the low temperature regime, primarily the pions, only produce significant corrections to the pressure in the low temperature regime where constituent quarks are frozen. Therefore, in addition to the corrections emerging from fluctuations of constant fields that lead to important corrections in the presence of the fermion sign problem, we have evaluated corrections due to fully dynamic pion and sigma meson fields.¹⁹ As soon as the pressure of quark degrees of freedom starts to rise at the chiral and deconfinement cross-over, mesonic pressure contributions become comparatively small.

The good agreement of the PNJL model at mean field level with lattice calculations remains in the presence of the mesonic corrections calculated in this work. The most prominent feature of the pressure, which is the steep rise near the critical temperature, is only slightly modified by the corrections due to dynamic fluctuations of pions and sigma mesons. Below the quark-antiquark threshold the pressure generated by pion fluctuations is basically the pressure of a free pion gas. As low temperatures are difficult to access by lattice QCD, the pressure in typical lattice calculations is normalised to zero at some finite temperature below T_c . This might explain why the pressure of the PNJL model including mesonic corrections is slightly higher than the pressure of the lattice calculations [8]. Due to these normalisation issues the comparison suffers from this uncertainty, $\Delta(p/T^4) = p/T^4|_{T=T_{\text{norm}}} - p/T^4|_{T\rightarrow 0}$, which in turn depends on the normalisation temperature T_{norm}

¹⁹However, no back-reaction of fluctuational effects on the mean field equations is taken into account.

and additionally on the realized pion mass. For large pion masses (see Fig. 11) this correction is small maintaining the good agreement between PNJL and lattice results. For small pion masses the pressure contribution from pion modes is almost flat in the temperature region $T \approx m_\pi$, such that the pressure from lattice and PNJL calculations mainly differ by a shift in p/T^4 . Shifting the lattice data to higher values of p/T^4 indeed reduces the difference between Stefan-Boltzmann limit and lattice data for the pressure at high temperatures around $2-3T_c$ and above, improving the agreement between lattice results and PNJL. Even when taking into account these issues in the comparison of PNJL and lattice results, we conclude that there exists a good qualitative and quantitative agreement of these two approaches.

The fluctuation corrections derived and evaluated in this work predominate in quantities for which mean field contributions cancel, e.g. selected susceptibilities. Thus the effects of the corrections beyond mean field on the off-diagonal (isovector) susceptibilities already evaluated in lattice QCD [8] and in previous NJL model studies [15], are of particular interest for future investigations.

References

- [1] Z. Fodor and S. D. Katz, JHEP **0203**, 014 (2002) [arXiv:hep-lat/0106002].
- [2] Z. Fodor, S. D. Katz and K. K. Szabo, Phys. Lett. B **568**, 73 (2003) [arXiv:hep-lat/0208078].
- [3] P. de Forcrand and O. Philipsen, Nucl. Phys. B **642**, 290 (2002) [arXiv:hep-lat/0205016].
- [4] P. de Forcrand and O. Philipsen, Nucl. Phys. B **673**, 170 (2003) [arXiv:hep-lat/0307020].
- [5] C. R. Allton *et al.*, Phys. Rev. D **66**, 074507 (2002) [arXiv:hep-lat/0204010].
- [6] C. R. Allton, S. Ejiri, S. J. Hands, O. Kaczmarek, F. Karsch, E. Laermann and C. Schmidt, Phys. Rev. D **68**, 014507 (2003) [arXiv:hep-lat/0305007].
- [7] S. Ejiri, T. Hatsuda, N. Ishii, Y. Maezawa, N. Ukita, S. Aoki and K. Kanaya, arXiv:hep-lat/0609075.
- [8] C. R. Allton *et al.*, Phys. Rev. D **71**, 054508 (2005) [arXiv:hep-lat/0501030].
- [9] G. Boyd, J. Engels, F. Karsch, E. Laermann, C. Legeland, M. Lutgemeier and B. Petersson, Nucl. Phys. B **469**, 419 (1996) [arXiv:hep-lat/9602007].
- [10] O. Kaczmarek, F. Karsch, P. Petreczky and F. Zantow, Phys. Lett. B **543**, 41 (2002) [arXiv:hep-lat/0207002].
- [11] G. Boyd, S. Gupta, F. Karsch, E. Laermann, B. Petersson and K. Redlich, Phys. Lett. B **349**, 170 (1995) [arXiv:hep-lat/9501029].
- [12] K. Fukushima, Phys. Lett. B **553**, 38 (2003) [arXiv:hep-ph/0209311]. K. Fukushima, Phys. Rev. D **68**, 045004 (2003) [arXiv:hep-ph/0303225].

- [13] K. Fukushima, Phys. Lett. B **591**, 277 (2004) [arXiv:hep-ph/0310121]; Y. Hatta and K. Fukushima, Phys. Rev. D **69**, 097502 (2004) [arXiv:hep-ph/0307068].
- [14] C. Ratti, M. A. Thaler and W. Weise, Phys. Rev. D **73**, 014019 (2006) [arXiv:hep-ph/0506234].
- [15] C. Sasaki, B. Friman and K. Redlich, Phys. Rev. D **75**, 054026 (2007) [arXiv:hep-ph/0611143].
- [16] C. Sasaki, B. Friman and K. Redlich, Phys. Rev. D **75**, 074013 (2007) [arXiv:hep-ph/0611147].
- [17] S. K. Ghosh, T. K. Mukherjee, M. G. Mustafa and R. Ray, Phys. Rev. D **73**, 114007 (2006) [arXiv:hep-ph/0603050].
- [18] S. Mukherjee, M. G. Mustafa and R. Ray, arXiv:hep-ph/0609249.
- [19] Z. Zhang and Y. X. Liu, arXiv:hep-ph/0610221.
- [20] S. Rößner, C. Ratti and W. Weise, Phys. Rev. D **75**, 034007 (2007) [arXiv:hep-ph/0609281].
- [21] C. Ratti, S. Rößner, M. A. Thaler and W. Weise, Eur. Phys. J. C **49**, 213 (2007) [arXiv:hep-ph/0609218].
- [22] K. Fukushima, arXiv:0803.3318 [hep-ph].
- [23] A. Dumitru, R. D. Pisarski and D. Zschesche, Phys. Rev. D **72**, 065008 (2005) [arXiv:hep-ph/0505256].
- [24] F. Karsch, E. Laermann and A. Peikert, Nucl. Phys. B **605**, 579 (2001) [arXiv:hep-lat/0012023].
- [25] O. Kaczmarek and F. Zantow, Phys. Rev. D **71**, 114510 (2005) [arXiv:hep-lat/0503017].
- [26] C. Ratti, S. Rößner and W. Weise, Phys. Lett. B **649**, 57 (2007) [arXiv:hep-ph/0701091].
- [27] S. P. Klevansky, Rev. Mod. Phys. **64**, 649 (1992).
- [28] T. Hatsuda and T. Kunihiro, Phys. Rept. **247**, 221 (1994) [arXiv:hep-ph/9401310].
- [29] M. Lutz, S. Klimt and W. Weise, Nucl. Phys. A **542**, 521 (1992); U. Vogl and W. Weise, Prog. Part. Nucl. Phys. **27**, 195 (1991).
- [30] H. Hansen, W. M. Alberico, A. Beraudo, A. Molinari, M. Nardi and C. Ratti, Phys. Rev. D **75**, 065004 (2007) [arXiv:hep-ph/0609116].
- [31] J. Hüfner, S. P. Klevansky, P. Zhuang and H. Voss, Annals Phys. **234**, 225 (1994).
- [32] D. Blaschke, M. Buballa, A. E. Radzhabov and M. K. Volkov, arXiv:0705.0384 [hep-ph].